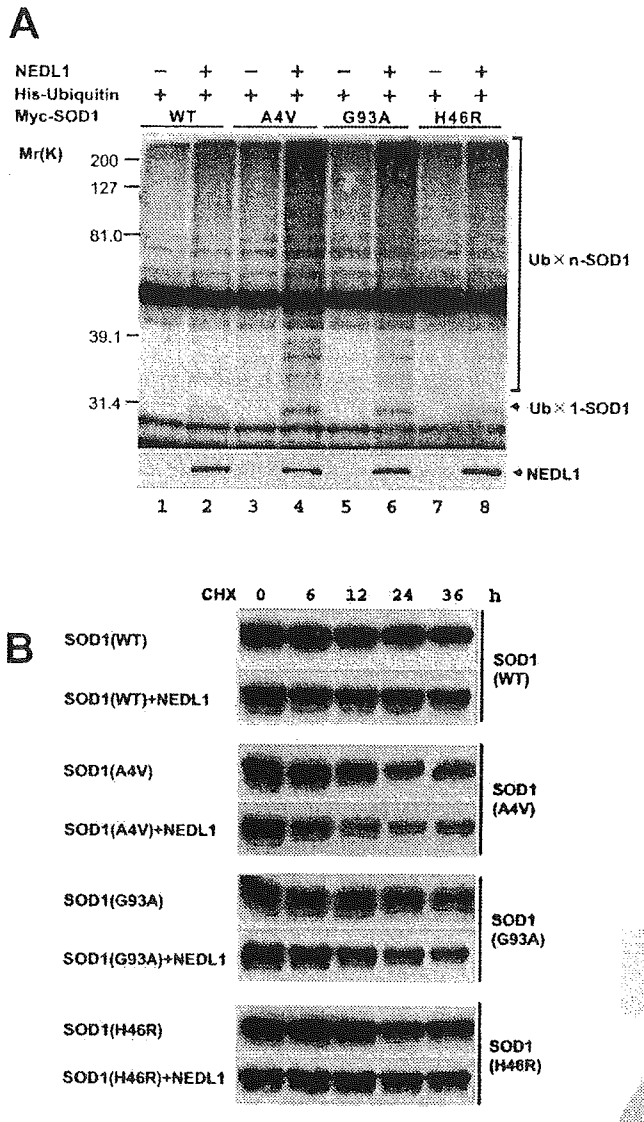

FIG. 4. **NEDL1-dependent ubiquitination and degradation of mutant forms of SOD1 correlate broadly with their respective clinical phenotypes.** *A*, NEDL1 ubiquitinates mutant SOD1 in a mutant type-dependent manner. COS-7 cells were transiently cotransfected with the indicated expression plasmids. Whole cell lysates from transfected COS-7 cells were immunoprecipitated with anti-Myc antibody, and immunoprecipitates were analyzed by Western blotting with anti-ubiquitin (*Ub*) antibody (*upper panel*). The *bracket* indicates slowly migrating ubiquitinated forms of SOD1. Whole cell lysates were analyzed by immunoblotting with anti-NEDL1 antibody to confirm the expression of transfected NEDL1 (*lower panel*). The running positions of molecular weight markers are indicated on the left. *B*, half-lives of wild-type (*WT*) and mutant SOD1 proteins in the presence or absence of NEDL1. Cell lysates were harvested from Neuro2a cells transfected with *SOD1* alone or with *SOD1* plus *NEDL1* at different time points as indicated after the addition of cycloheximide (*CHX*; final concentration of 50 μg/ml) and were analyzed for SOD1 protein levels by Western blotting with anti-FLAG antibody. In the presence of NEDL1, the half-lives of various mutant SOD1 proteins were reduced also roughly dependent on the disease severity of FALS (A4V > G93A > H46R).

Immunohistochemistry—One of the characteristic cytopathological changes of mutant SOD1-linked FALS is the formation of neuronal Lewy body-like hyaline inclusions (LBHIs) that contain aggregates of SOD1 and ubiquitin (24). We therefore performed immunostaining to determine whether the NEDL1 protein is included within the LBHIs of the spinal cord motor

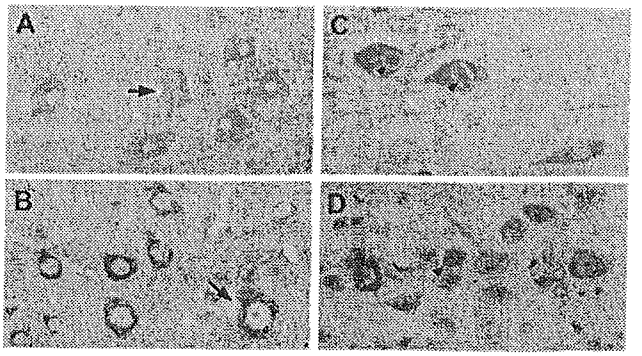

FIG. 5. **NEDL1 immunohistochemical analyses.** *A*, immunohistochemical analysis of NEDL1 in normal human spinal cord. NEDL1-positive anterior horn cells are evident (*arrow*), although the immunoreactivity for NEDL1 is somewhat faint. There was no counterstaining. Magnification ×520. *B*, NEDL1 immunohistochemistry in normal mouse spinal cord. Normal anterior horn cells are positive for NEDL1 (*arrow*). The section was counterstained with hematoxylin. Magnification ×750. *C*, immunostaining for NEDL1 in spinal cord LBHIs from an FALS patient with a frameshift 126 mutation in the *SOD1* gene. The NEDL1-positive reaction products were mostly restricted to the cores of the core and halo-type LBHIs (*arrowheads*). In the LBHI-bearing neurons and residual neurons, the antibody to NEDL1 also stained the neuronal cell body. There was no counterstaining. Magnification ×540. *D*, NEDL1 immunostaining in a spinal cord LBHI from an SOD1(H46R) transgenic mouse. An ill defined LBHI in the SOD1(H46R) transgenic mouse was positive for NEDL1; this ill defined LBHI shows a diffuse staining pattern (*arrowhead*). The staining intensity in the residual neurons stained by anti-NEDL1 antibody varied from neuron to neuron. The section was counterstained with hematoxylin. Magnification ×770.

neurons obtained from two siblings with FALS caused by frameshift 126 mutation of SOD1 (11, 12). One case had neuropathological findings compatible with FALS with posterior column involvement, whereas the other had multisystem degeneration in addition to motor neuron disturbance. We also performed NEDL1 immunostaining in specimens obtained from mutant SOD1(H46R) transgenic mice at 180 days, by which time they show clinical motor signs in the hind limbs (13). The specificity of the NEDL1 staining was confirmed by pretreating the specimens with an excess of NEDL1 antigen. NEDL1 immunoreactivity in the spinal cords of the human control cases was identical to that of normal mice: immunoreactivity was identified predominantly in the cytoplasm of the neurons of the spinal cords (Fig. 5, *A* and *B*). The LBHIs in the anterior horn cells of two FALS patients and transgenic mice showed equivalent immunoreactivity for NEDL1. Although the intensity of NEDL1 immunoreactivity in neuronal LBHIs varied, most of the LBHIs were immunoreactive for NEDL1 (Fig. 5, *C* and *D*). The reaction products were generally restricted to the cores of the core and halo-type LBHIs that showed eosinophilic cores with pale peripheral halos upon hematoxylin and eosin staining (Fig. 5*C*); by contrast, immunopositive NEDL1 in ill defined LBHIs was distributed throughout the inclusions (Fig. 5*D*). NEDL1 immunoreactivity in the residual neurons in humans and mice was identified primarily in cell bodies. Thus, NEDL1 immunostaining was clearly positive in the FALS-related LBHIs that were also positive for ubiquitin and SOD1 (data not shown).

NEDL1 Targets Dishevelled-1 for Ubiquitin-mediated Protein Degradation—We next hypothesized that the physiological function of NEDL1 to mediate ubiquitination is interfered with by mutant SOD1. To test this hypothesis, we again performed yeast two-hybrid screening to obtain NEDL1-interacting molecules using the large region of NEDL1 (amino acids 382–1448) as bait. Of 396 His and β-galactosidase double-positive clones, 282 clones were subjected to DNA sequencing, and we identi-

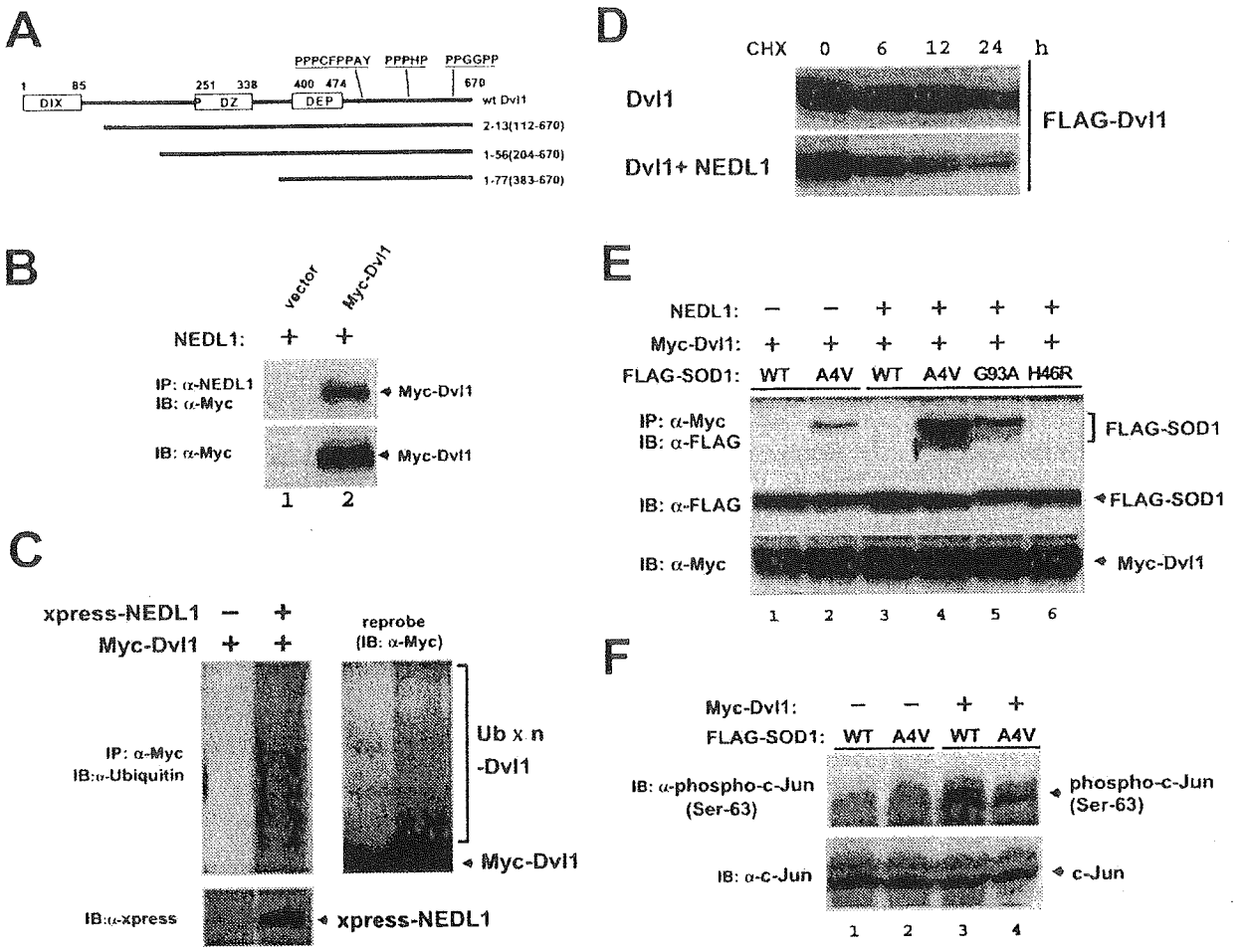

FIG. 6. **Dvl1 is a substrate of NEDL1, and its functions are disturbed by mutant SOD1(A4V).** *A*, schematic illustration of full-length Dvl1 and three clones obtained by yeast two-hybrid screening. Human Dvl1 consists of 670 amino acids and contains three conserved domains, including the DIX, PDZ, and DEP domains. Between the DEP domain and the C-terminal end, there are three proline-rich clusters, which might act as WW domain recognition sites. All three clones (clones 2–13, 1–56, 1–77) contain the DEP domain and these clusters. *B*, NEDL1 interacts with Dvl1. Myc-tagged Dvl1 was overexpressed together with NEDL1 in Neuro2a cells. Whole cell lysates were immunoprecipitated (*IP*) with anti-NEDL1 antibody, followed by immunoblotting (*IB*) with anti-Myc antibody (*upper panel*). The expression levels of Myc-tagged Dvl1 were analyzed by immunoblotting using anti-Myc antibody (*lower panel*). *C*, NEDL1 ubiquitinates Dvl1 in Neuro2a cells. The cells were transiently transfected with the indicated expression plasmids along with the ubiquitin expression plasmid in the presence or absence of the expression plasmid for XPRESS-tagged NEDL1. Whole cell lysates were immunoprecipitated with anti-Myc antibody and then immunoblotted with anti-ubiquitin antibody (*left panel*). The ladder of bands denoted by the *bracket* appeared to be ubiquitinated Dvl1. The expression of XPRESS-NEDL1 was analyzed by immunoblotting using anti-XPRESS antibody. The membrane was reprobed with anti-Myc antibody (*right panel*). *D*, Dvl1 is degraded by NEDL1. Neuro2a cells were transfected with the expression plasmid for FLAG-tagged Dvl1 with or without the NEDL1 expression plasmid. Transfected cells were harvested at different time points as indicated after the addition of cycloheximide (*CHX*; final concentration of 50 μg/ml), and Dvl1 protein levels were analyzed by Western blotting with anti-FLAG antibody. In the presence of NEDL1, the half-lives of FLAG-Dvl1 were significantly reduced. *E*, Dvl1 binds to mutant SOD1(A4V), and the degree of its binding is enhanced in the presence of NEDL1. Whole cell lysates prepared from COS-7 cells transfected with the indicated combinations of expression plasmids were subjected to immunoprecipitation and Western analyses as indicated. *F*, c-Jun phosphorylation by overexpression of Dvl1 is suppressed upon coexpression of mutant SOD1(A4V). Whole cell lysates from COS-7 cells transfected with the indicated combinations of expression plasmids were subjected to Western blotting with antibody against the phosphorylated form of c-Jun (*upper panel*) or with anti-c-Jun antibody (*lower panel*). *wt/WT*, wild-type.

fied Dvl1 (three clones). Human Dvl1 is a 670-amino acid protein with three conserved domains: a DIX domain, which is required for canonical Wnt/T-cell factor signaling; a PDZ domain, which is a target of both Stbm and casein kinase I binding; and a DEP domain, which is responsible for Dvl membrane localization during planar cell polarity signaling (25–27). Between the DEP domain and C-terminal end, there are three proline-rich clusters unique to mammalian Dvl1, which presumably act as the WW domain recognition sites. All three clones (clones 2–13, 1–56, and 1–77) contain the DEP domain and proline-rich clusters, suggesting that NEDL1 interacted with Dvl1 in the C-terminal half (Fig. 6*A*). In Neuro2a cells, NEDL1 co-immunoprecipitated with Dvl1 (Fig. 6*B*) and ubiquitinated it for degradation (Fig. 6, *C* and *D*). Thus, Dvl1 may be one of the physiological targets of NEDL1 E3. As recent studies strongly suggest that the cytotoxicity of SOD1 mutants is responsible for their aggregate properties, incorporating other proteins essential for cells into their aggregates (28), we examined the association between mutant SOD1 and Dvl1, both of which interact with NEDL1. Of interest, Dvl1 bound to mutant SOD1(A4V), and complex formation was increased in the presence of NEDL1 roughly proportionately to the disease severity of FALS caused by the particular SOD1 mutant (Fig. 6*E*). Dvl1 is known to transduce not only the Wnt/β-catenin/T-cell factor pathway, but also the JNK/c-Jun pathway (27). Therefore, we next examined whether the Dvl1-induced phos-

phorylation of c-Jun at Ser^{63} was affected by the tight complex formation induced by inclusion of mutant SOD1. As shown in Fig. 6*F*, c-Jun phosphorylation induced by overexpression of Dvl1 was significantly suppressed by coexpression with mutant SOD1(A4V) in COS-7 cells.

DISCUSSION

Our present results demonstrate that a novel HECT-type NEDL1 E3, which is preferentially expressed in neuronal tissues, specifically targets mutant forms of SOD1 for ubiquitination-mediated protein degradation. NEDL1 is also associated with TRAP-δ localized at the ER translocon. The TRAP complex has recently been shown to facilitate the initiation of protein translocation in a substrate-specific manner (29). The NEDL1·TRAP-δ complex recognizes mutant (but not wild-type) SOD1, with a binding intensity that broadly parallels the disease severity of FALS. NEDL1 immunoreactivity was detected in the FALS-related LBHIs in the spinal cord ventral horn motor neurons, suggesting that, although mutant SOD1 is ubiquitinated for degradation by NEDL1, the mutant SOD1·NEDL1·TRAP-δ complex aggregates within the LBHIs. It is also conceivable that fragmentation of the Golgi apparatus reported in ALS patients and transgenic mice might be related to this aggregation (30, 31). These findings suggest possible hypotheses for the role of NEDL1 in the pathogenesis of FALS: 1) NEDL1, alone or with TRAP-δ, ubiquitinates and aggregates mutant SOD1, thereby decreasing the function of mutant SOD1; 2) NEDL1 and TRAP-δ form aggregates with mutant SOD1 that induce fragmentation of the Golgi apparatus, leading to neuronal apoptosis; 3) formation of these aggregates causes dysfunction of NEDL1 and/or TRAP-δ, and this, in turn, induces disturbances that ultimately cause motor neuron death; and 4) the mutant SOD1·NEDL1·TRAP-δ aggregates trap and inactivate unknown factor(s) such as molecular chaperones whose normal function is important for motor neuron viability.

To further understand the role of NEDL1 in motor neuron death, we searched for the physiological targets of NEDL1 and identified Dvl1. As expected, Dvl1 is ubiquitinated for degradation by NEDL1. Surprisingly, however, Dvl1 also interacts with mutant SOD1 in the presence of NEDL1 roughly proportionately to the disease severity of FALS caused by the particular SOD1 mutant. Dvl1, an essential multimodule signal transducer localized in the cellular cytosol and cytoskeleton, mediates planar cell polarity signaling as well as canonical Wnt/β-catenin signaling (27, 32). In mammals, three Dvl family members have so far been reported, and the level of Dvl1 expression is high in neuronal tissues (33). As far as we know, NEDL1 is the first E3 for Dvl1, interacting with the C-terminal region containing three proline-rich clusters. A recent report suggests that Dvl1 regulates microtubule stability through inhibition of glycogen synthase kinase-3β (34). Because cytoskeletal abnormalities have been reported in ALS motor neurons (35), it is possible that the effect of mutant SOD1 on NEDL1-mediated Dvl1 degradation is involved in the motor neuron death. Furthermore, Dvl1 is abundant in the postsynaptic membrane region at the neuromuscular junction (36) that is reported to be involved in several neurodegenerative disorders (37, 38). Of interest, *Dvl1* is mapped to chromosome 1p36, which is a commonly deleted region in many human cancers, including neuroblastoma (39). As NEDL1 is highly expressed in neuroblastomas with favorable prognosis, which have a tendency to differentiate and/or regress, NEDL1 may be involved in the regulation of neuronal differentiation and survival possibly by controlling Dvl1.

NEDL1, TRAP-δ, mutant SOD1, and Dvl1 appear to form a complex roughly proportionately to the disease severity of FALS caused by the particular SOD1 mutant. Our present observations strongly suggest that NEDL1 may be a quality control E3 recognizing misfolded mutant SOD1 (40). The association between mutant SOD1 and NEDL1 may induce the conformational change in the NEDL1 protein to increase the binding intensity with other physiological targets such as TRAP-δ (not ubiquitinated) and Dvl1 (ubiquitinated). This may lead to tight complex formation especially when the proteasome activity is impaired. It has been reported that the expression and function of proteasomes decrease with age in the spinal cord (7). Okado-Matsumoto and Fridovich (41) have also found that complex formation between mutant SOD1 and heat shock proteins leads to protein aggregates. Because our data show that the ER translocon component TRAP-δ is involved, aggregate formation may occur at the sites of the ER or Golgi apparatus or even at other cellular sites. The complex formation including NEDL1 and mutant SOD1 may conversely affect the physiological function of NEDL1, as demonstrated by a decrease in Dvl1-induced phosphorylation of c-Jun.

Recently, the RING finger-type E3 Dorfin has been reported to ubiquitinate mutant SOD1 for degradation (42). However, NEDL1 and Dorfin appear to be different in several aspects. First, NEDL1 is expressed specifically in neuronal tissues, including the spinal cord, whereas Dorfin is ubiquitously expressed in most human tissues. Second, both interaction between NEDL1 and mutant SOD1 and ubiquitination of the latter by NEDL1 roughly parallel the disease severity caused by the particular SOD1 mutant, whereas Dorfin similarly ubiquitinates mutant forms of SOD1. In addition, we have identified Dvl1 and TRAP-δ as cellular target proteins of NEDL1, whereas the physiological targets of Dorfin have never been reported. It is probable that there are some other E3 ligases targeting mutant SOD1. However, the molecular characteristics, including tissue-specific expression, subcellular localization, and age-dependent expression, might be important in the development of the FALS phenotype.

In conclusion, we have identified a novel neuronal E3 (NEDL1) that interacts with TRAP-δ and also binds to and ubiquitinates Dvl1 for degradation. Strikingly, NEDL1 targets and ubiquitinates mutant (but not wild-type) SOD1 for degradation. NEDL1 may normally function in the quality control of cellular proteins by eliminating misfolded proteins such as mutant SOD1, possibly via a mechanism analogous to that of ER-associated degradation (43–45). NEDL1 appears to complex tightly with mutant SOD1, Dvl1, and TRAP-δ, forming aggregates with species of mutant SOD1 that have escaped ubiquitin-mediated degradation. The NEDL1 function that affects the activities of the target proteins may also be modulated by mutant SOD1. All of these might contribute to the pathogenesis of FALS; further elucidation of the molecular mechanism of formation of this complex and its pathogenicity may provide insights into motor neuron death in ALS as well as possible new therapeutic strategies for ALS.

Acknowledgments—We thank Robert H. Brown, Jr. (Harvard Medical School) for critical comments and reading the manuscript. We also thank M. Ohira and Y. Nakamura for helping with cDNA cloning and sequencing; K. Watanabe and M. Suzuki for making plasmid constructs; M. Nagai and M. Kato for helping with immunohistochemical studies; S. Hatakeyama, M. Matsumoto, and K. Nakayama for ubiquitination assay instruction; and S. Sakiyama for reading the manuscript.

REFERENCES

1. Rosen, D. R., Siddique, T., Patterson, D., Figlewicz, D. A., Sapp, P., Hentati, A., Donaldson, D., Goto, J., O'Regan, J. P., Deng, H. X., Rahmani, Z., Krizus, A., McKenna-Yasek, D., Cayabyab, A., Gaston, S. M., Berger, R., Tanzi, R. E., Halperin, J. J., Herzfeldt, B., van den Bergh, R., Hung, W.-Y., Bird, T., Deng, G., Mulder, D. W., Smyth, C., Laing, N. G., Soriano, E., Pericak-Vance, M. A., Haines, J., Rouleau, G. A., Gusella, J. S., Horvitz, H. R., and Brown, R. H. (1993) *Nature* **364**, 59–62R. H.
2. Deng, H. X., Hentati, A., Tainer, J. A., Iqbal, Z., Cayabyab, A., Hung, W.-Y.,

Getzoff, E. D., Hu, P., Herzfeldt, B., Roos, R. P., Warner, C., Deng, G., Soriano, E., Smyth, C., Parge, H. E., Ahmed, A., Roses, A. D., Hallewell, R., Rericak-Vance, M. A., and Siddique, T. (1993) *Science* **261,** 1047–1051
3. Cleveland, D. W., and Liu, J. (2001) *Nat. Med.* **6,** 1320–1321
4. Brown, R. H., Jr., and Robberecht, W. (2001) *Semin. Neurol.* **21,** 131–139
5. Cluskey, S., and Ramsden, D. B. (2001) *Mol. Pathol.* **54,** 386–392
6. Orrell, R. W., and Figlewicz, D. A. (2001) *Neurology* **57,** 9–17
7. Keller, J. N., Huang, F. F., and Markesbery, W. R. (2000) *Neuroscience* **98,** 149–156
8. Hoffman, E. K., Wilcox, H. M., Scott, R. W., and Siman, R. (1996) *J. Neurol. Sci.* **139,** 15–20
9. Kunst, C. B., Mezey, E., Brownstein, M. J., and Patterson, D. (1997) *Nat. Genet.* **15,** 91–94
10. Hartmann, E., Gorlich, D., Kostka, S., Otto, A., Kraft, R., Knespel, S., Burger, E., Rapoport, T. A., and Prehn, S. (1993) *Eur. J. Biochem.* **214,** 375–381
11. Kato, S., Shimoda, M., Watanabe, Y., Nakashima, K., Takahashi, K., and Ohama, E. (1996) *J. Neuropathol. Exp. Neurol.* **55,** 1089–1101
12. Kato, S., Hayashi, H., Nakashima, K., Nanba, E., Kato, M., Hirano, A., Nakano, I., Asayama, K., and Ohama, E. (1997) *Am. J. Pathol.* **151,** 611–620
13. Nagai, M., Aoki, M., Miyoshi, I., Kato, M., Pasinelli, P., Kasai, N., Brown, R. H., Jr., and Itoyama, Y. (2001) *J. Neurosci.* **21,** 9246–9254
14. Nakagawara, A. (1998) *Med. Pediatr. Oncol.* **31,** 113–115
15. Harvey, K. F., and Kumar, S. (1999) *Trends Cell Biol.* **9,** 166–169
16. Kumar, S., Tomooka, Y., and Noda, M. (1992) *Biochem. Biophys. Res. Commun.* **30,** 1155–1161
17. Kato, S., Takikawa, M., Nakashima, K., Hirano, A., Cleveland, D. W., Kusaka, H., Shibata, N., Kato, M., Nakano, I., and Ohama, E. (2000) *Amyotroph. Lateral Scler. Other Motor Neuron Disorders* **1,** 163–184
18. Orrell, R. W. (2000) *Neuromuscul. Disorders* **10,** 63–68
19. Cudkowicz, M. E., McKenna-Yasek, D., Sapp, P. E., Chin, W., Geller, B., Hayden, D. L., Schoenfeld, D. A., Hosler, B. A., Horvitz, H. R., and Brown, R. H. (1997) *Ann. Neurol.* **41,** 210–221
20. Ratovitski, T., Corson, L. B., Strain, J., Wong, P., Cleveland, D. W., Culotta, V. C., and Borchelt, D. R. (1999) *Hum. Mol. Genet.* **8,** 1451–1460
21. Aoki, M., Ogasawara, M., Matsubara, Y., Narisawa, K., Nakamura, S., Itoyama, Y., and Abe, K. (1993) *Nat. Genet.* **5,** 323–324
22. Kato, M., Aoki, M., Ohta, M., Nagai, M., Ishizaki, F., Nakamura, S., and Itoyama, Y. (2001) *Neurosci. Lett.* **312,** 165–168
23. Andersen, P. M., Forsgren, L., Binzer, M., Nilsson, P., Ala-Hurula, V., Keranen, M. L., Bergmark, L., Saarinen, A., Haltia, T., Tarvainen, I., Kinnunen, E., Udd, B., and Marklund, S. L. (1996) *Brain* **119,** 1153–1172
24. Shibata, N., Hirano, A., Kobayashi, M., Siddique, T., Deng, H. X., Hung, W.-Y., Kato, T., and Asayama, K. (1996) *J. Neuropathol. Exp. Neurol.* **55,** 481–490
25. Sussman, D. J., Klingensmith, J., Salinas, P., Adams, P. S., Nusse, R., and Perrimon, N. (1994) *Dev. Biol.* **166,** 73–86
26. Wodarz, A., and Nusse, R. (1998) *Annu. Rev. Cell Dev. Biol.* **14,** 59–88
27. Boutros, M., Paricio, N., Strutt, D. I., and Mlodzik, M. (1998) *Cell* **94,** 109–118
28. Julien, J. P. (2001) *Cell* **104,** 581–591
29. Fons, R. D., Bogert, B. A., and Hegde, R. S. (2003) *J. Cell Biol.* **160,** 529–539
30. Fujita, Y., Okamoto, K., Sakurai, A., Gonatas, N. K., and Hirano, A. (2000) *J. Neurol. Sci.* **174,** 137–140
31. Mourelatos, Z., Gonatas, N. K., Stieber, A., Gurney, M. E., and Dal Canto, M. C. (1996) *Proc. Natl. Acad. Sci. U. S. A.* **93,** 5472–5477
32. Wharton, K. A., Jr. (2003) *Dev. Biol.* **253,** 1–17
33. Tsang, M., Lijam, N., Yang, Y., Beier, D. R., Wynshaw-Boris, A., and Sussman, D. J. (1996) *Dev. Dyn.* **207,** 253–262
34. Krylova, O., Messenger, M. J., and Salinas, P. C. (2000) *J. Cell Biol.* **151,** 83–94
35. Julien, J. P., and Beaulieu, J. M. (2000) *J. Neurol. Sci.* **180,** 7–14
36. Luo, Z. G., Wang, Q., Zhou, J. Z., Wang, J., Luo, Z., Liu, M., He, X., Wynshaw-Boris, A., Xiong, W. C., Lu, B., and Mei, L. (2002) *Neuron* **35,** 489–505
37. De Ferrari, G. V., and Inestrosa, N. C. (2000) *Brain Res. Brain Res. Rev.* **33,** 1–12
38. Kaytor, M. D., and Orr, H. T. (2000) *Curr. Opin. Neurobiol.* **12,** 275–278
39. Versteeg, R., Caron, H., Cheng, N. C., van der Drift, P., Slater, R., Westerveld, A., Voute, P. A., Delattre, O., Laureys, G., van Roy, N., and Speleman, F. (1995) *Eur. J. Cancer* **31,** 538–541
40. Murata, S., Minami, Y., Minami, M., Chiba, T., and Tanaka, K. (2001) *EMBO Rep.* **2,** 1133–1138
41. Okado-Matsumoto, A., and Fridovich, I. (2002) *Proc. Natl. Acad. Sci. U. S. A.* **99,** 9010–9014
42. Niwa, J., Ishigaki, S., Hishikawa, N., Yamamoto, M., Doyu, M., Murata, S., Tanaka, K., Taniguchi, N., and Sobue, G. (2002) *J. Biol. Chem.* **277,** 36793–36798
43. Mori, K. (2000) *Cell* **101,** 451–454
44. Travers, K. J., Patil, C. K., Wodicka, L., Lockhart, D. J., Weissman, J. S., and Walter, P. (2000) *Cell* **101,** 249–258
45. Wickner, S., Maurizi, M. R., and Gottesman, S. (1999) *Science* **286,** 1888–1893

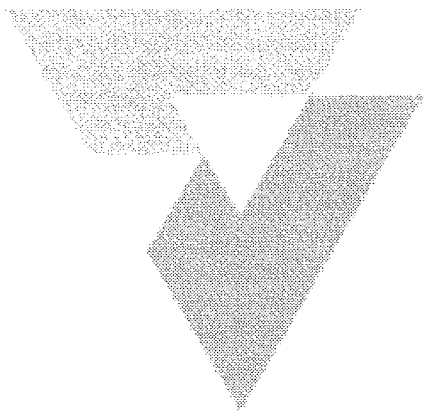

ACADEMIC PRESS

Available online at www.sciencedirect.com

SCIENCE DIRECT®

Biochemical and Biophysical Research Communications 303 (2003) 496–503

BBRC

www.elsevier.com/locate/ybbrc

Mutant SOD1 linked to familial amyotrophic lateral sclerosis, but not wild-type SOD1, induces ER stress in COS7 cells and transgenic mice☆

Shinsuke Tobisawa,[a,b] Yasukazu Hozumi,[b] Shigeki Arawaka,[a] Shingo Koyama,[a] Manabu Wada,[a] Makiko Nagai,[c] Masashi Aoki,[c] Yasuto Itoyama,[c] Kaoru Goto,[b] and Takeo Kato[a,*]

[a] *Third Department of Internal Medicine, Yamagata University School of Medicine, 2-2-2 Iida-Nishi, Yamagata 990-9585, Japan*
[b] *Department of Anatomy and Cell Biology, Yamagata University School of Medicine, Yamagata, Japan*
[c] *Department of Neurology, Tohoku University School of Medicine, Seidai, Japan*

Received 21 February 2003

Abstract

Mutations in a Cu, Zn-superoxide dismutase (SOD1) cause motor neuron death in human familial amyotrophic lateral sclerosis (FALS) and its mouse model, suggesting that mutant SOD1 has a toxic effect on motor neurons. However, the question of how the toxic function is gained has not been answered. Here, we report that the mutant SOD1s linked to FALS, but not wild-type SOD1, aggregated in association with the endoplasmic reticulum (ER) and induced ER stress in the cDNA-transfected COS7 cells. These cells showed an aberrant intracellular localization of mitochondria and microtubules, which might lead to a functional disturbance of the cells. Motor neurons of the spinal cord in transgenic mice with a FALS-linked mutant SOD1 also showed a marked increase of GRP78/BiP, an ER-resident chaperone, just before the onset of motor symptoms. These data suggest that ER stress is involved in the pathogenesis of FALS with an SOD1 mutation.

Keywords: Superoxide dismutase 1; Amyotrophic lateral sclerosis; Endoplasmic reticulum

Amyotrophic lateral sclerosis (ALS) is a neurodegenerative disease characterized by a selective loss of motor neurons in the motor cortex, brainstem, and spinal cord. Patients with ALS show progressive muscle weakness, atrophy, and, ultimately, death due to respiratory failure, which usually occurs within 3–5 years of the onset of the disease. In most cases, ALS occurs sporadically; however, there is a family history of the disease in 5–10% of the cases (familial ALS: FALS). It is known that approximately 20% of FALS is caused by a missense mutation of the Cu, Zn-superoxide dismutase (SOD1) gene [1,2]. FALS with an SOD1 mutation shows an adult-onset, autosomal dominant form of ALS. Until now, FALS-linked SOD1 mutations have been reported to occur at about 60 sites of the amino acid sequence of SOD1 (http://www.alsod.org) [3]. At first, a diminished superoxide scavenging activity of SOD1 mutant and subsequent oxidative stress were considered to be a pathogenic mechanism of FALS with an SOD1 mutation [1,2,4–6]. However, elimination of SOD1 in a knock-out mouse model did not cause any neurological symptoms or pathology [7]. Moreover, transgenic mice with a FALS-linked mutated SOD1 gene developed motor neuron symptoms and pathology irrespective of the degree of enzymatic activity of SOD1 [8–11]. In FALS patients, the age at the onset and the severity of the disease have no relationship to the degree of enzymatic activity of SOD1 [12–14]. Therefore, the functional loss

☆ *Abbreviations:* ALS, amyotrophic lateral sclerosis; ER, endoplasmic reticulum; FALS, familial amyotrophic lateral sclerosis; PBS, phosphate-buffered saline; SOD1, superoxide dismutase 1.

* Corresponding author. Fax: +81-23-628-5318.
E-mail address: tkato@med.id.yamagata-u.ac.jp (T. Kato).

0006-291X/03/$ - see front matter © 2003 Elsevier Science (USA). All rights reserved.
doi:10.1016/S0006-291X(03)00353-X

of SOD1 does not seem to be the pathogenesis of FALS with an SOD1 mutation [15]. Another hypothesis is a possible toxic function of the mutant SOD1, in which the mutant obtains an aberrant catalytic ability. This includes the peroxynitrate and the peroxidase hypotheses [16,17]. In the former, the mutation of SOD1 was speculated to disrupt the active-site pocket of the enzyme to allow the copper to react with peroxynitrite, resulting in the nitration of proteins [16]. In the latter, the FALS-associated mutant SOD1 has been shown in vitro to augment the catalytic oxidation of a model substrate by hydrogen peroxide [17]. However, these hypotheses are not supported by the observation that the elevation or elimination of wild-type SOD1 has no effect on the symptoms or pathology of a transgenic mouse model with FALS-linked mutant SOD1 [15].

It is known that misfolding of a protein after biosynthesis results in aggregation of the protein, which causes damage of cells including neurons [18–20]. In a transgenic mouse with mutated SOD1, formation of insoluble, high-molecular-weight complexes of mutated SOD1 was observed several months before the onset of the disease [21]. In this report, the FALS-linked mutant SOD1 transfected to COS7 cells induces endoplasmic reticulum (ER) stress by the accumulation of insoluble, mutant SOD1 and a possible dysfunction of the intracellular transport, which may explain how the mutant SOD1 causes the disease. Similar changes of the ER are also observed in transgenic mice with a mutant SOD1.

Experimental procedures

Plasmid constructs. Total RNA was extracted from human white blood cells by acid guanidinium thiocyanate–phenol–chloroform extraction. First-strand cDNA was prepared using the 1st-Strand cDNA Synthesis kit for RT-PCR (AMV) (Roche Molecular Biochemicals, Mannheim, Germany). A full-length wild-type SOD1 cDNA with *Eco*RI linker sequences was generated by polymerase chain reaction (PCR) using a primer pair of a sense primer (5′-CGGAATTCA TGGCGACGAAGGCCGTGTG-3′) and an anti-sense primer (5′-GG GAATTCTTATTGGGCGATCCCA-3′) followed by subcloning into the *Eco*RI-cleaved pcDNA3 with an epitope tag composed of eight amino acids (FLAG marker peptide, Asp–Tyr–Lys–Asp–Asp–Asp–Lys; Eastman Kodak) that was fused to wild-type SOD1 by cloning the 24 base pairs of the FLAG coding sequence upstream to the coding region of wild-type SOD1 cDNA. PCR amplification was performed by using Ex *Taq* DNA polymerase (Takara Shuzo Tokyo, Japan) according to the following schedule: 94 °C for 30 s, 60 °C for 30 s, and 72 °C for 90 s for 30 cycles. Mutant SOD1 cDNAs were generated by site-specific mutagenesis. Wild-type and mutant SOD1s were also subcloned with FLAG coding sequence into pEF-BOS, which utilizes the human polypeptide chain elongation factor 1α promoter (EF-1α) [22]. Rat diacylglycerol kinase ζ (DGK ζ) cDNA [23] was subcloned into pEGFP-C2 (Clontech, Palo Alto, CA, USA). These subcloned cDNAs were sequenced by the Model 310 Autosequencer (Applied Biosystems, Foster City, CA, USA).

Cell culture and transfection. COS7 cells were cultured in Dulbecco's modified Eagle's medium with 10% fetal bovine serum and transfected with 1 μg or co-transfected with 2 μg (1 μg each) of plasmid DNA using Lipofectamine 2000 (Invitrogen, Carlsbad, CA, USA) according to the manufacturer's instructions. Cultured cells were harvested 48 h after transfection and lysed by sonication in a lysis buffer containing 50 mM Tris–HCl (pH 7.6), 150 mM NaCl, 5 mM EDTA, 1 mg/L leupeptin, and 50,000 U/L trasylol. After removal of undisrupted cells by centrifugation (5000*g*, 7 min, 4 °C), the resultant supernatant was designated as the *total lysate*. Protein concentrations were determined by the bicinchoninate method. Cytosol fraction was prepared according to the following method: the supernatant resulting from the removal of nuclear fraction by centrifugation (14,000*g*, 10 min, 4 °C) was ultracentrifuged (100,000*g*, 1 h, 4 °C). The resultant supernatant was designated as the *cytosol fraction*. The *pellet* was resuspended in a lysis buffer that equaled the cytosol fraction in volume.

Immunoblotting. The total lysate from COS7 cells was prepared as described above. Ten micrograms of total protein boiled for 5 min in a 3 × SDS sample buffer (New England Biolabs, Beverly, MA, USA) was subjected to 15% SDS–polyacrylamide gel electrophoresis. The separated proteins were then electrophoretically transferred onto a PolyScreen-PVDF membrane (NEN TM Life Science Products, USA). After blocking non-specific binding sites in 5% skim milk (w/v) in phosphate-buffered saline (PBS) with 0.01% Tween 20, the membrane was incubated for 1 h at room temperature with the antibody against FLAG or GRP78/BiP and then treated with peroxidase-conjugated anti-mouse or anti-rabbit IgG antibodies for 1 h. The immunoreactive bands were detected using a chemi-luminescence detection kit (ECL Western blotting kit, Amersham, Uppsala, Sweden). The cytosol and pellet fractions were prepared as described above. Ten microliters each of both fractions and total lysate were subjected to immunoblotting and the immunoreactive bands were detected using the same methods as described above.

Immunocytochemistry of cDNA-transfected COS7 cells. After transfection and a 24-h incubation, cells were fixed in 4% paraformaldehyde in a 0.1 M sodium phosphate buffer (pH 7.2), followed by a 0.1% Triton X-100 permeabilization for 5 min. After fixation, cells were washed extensively in PBS and blocked with PBS containing 5% normal goat serum (NGS) for 15 min. The cells were incubated with the following appropriate primary antibodies diluted in PBS containing 5% NGS: mouse anti-FLAG (M2) antibody (1 μl/ml, Sigma-Aldrich, St. Louis, MO, USA), rabbit anti-GRP78/BiP antibodies (diluted 1:1000, Stressgen), rabbit anti-SOD2 antibodies (diluted 1:10,000, provided by Dr. K. Asayama, University of Occupational and Environmental Health, Japan), and rabbit anti-tubulin antibodies (diluted 1:10,000, provided by Dr. R. Kuwano, Niigata University, Japan) for 1 h at room temperature. Cells were washed for 5 × 5 min in PBS and incubated with the following appropriate secondary antibodies diluted in PBS containing 5% NGS: anti-mouse IgG conjugated to Alexa 546 (diluted 1:250, Molecular Probes, Eugene, OR, USA) and biotinylated anti-rabbit IgG (diluted 1:250, Vector Laboratories, Burlingame, CA, USA) for 30 min at room temperature. Cells incubated with biotinylated anti-rabbit IgG antibodies were washed 5 × 5 times in PBS and incubated with streptavidin conjugated to Alexa 488 (10 μg/ml) for 30 min at room temperature. Cells were counterstained with the following markers for organelle and cytoskeleton according to the manufacturer's instructions: ER-Tracker (endoplasmic reticulum; ER marker, Molecular Probes), BODIPY FL-C5 ceramide (Golgi marker, Molecular Probes), and Alexa Fluor TM 568 phalloidin (Actin marker, Molecular Probes). Transfected cells with SOD1s in pcDNA3 were incubated with or without 10 μM lactacystin for 24 h. Stained cells were observed using a laser scanning confocal microscope (LSM 5 PASCAL, Zeiss, Germany).

Immunohistochemistry of transgenic mice with mutated SOD1. Formalin-fixed, paraffin-embedded tissue sections of the spinal cord were used from two lines of transgenic mice with SOD1 mutations, L84V (M. Kato, et al. Transgenic mice with ALS-linked SOD1 mutant L84V. Abstract of the 31st Annual Meeting of Society for Neuroscience, San Diego, 2001) and H46R (M. Nagai, et al. Transgenic mice with ALS-linked SOD1 mutant H46R. Abstract of the 30th Annual Meeting of Society for Neuroscience, 2000) and age-matched

non-transgenic mice. Deparaffinized sections were incubated with 1% hydrogen peroxide for 15 min, followed by 10% normal goat serum. The sections were subsequently incubated with anti-GRP78/BiP antibodies (diluted 1:1000, Stressgen, Victoria, BC, Canada) at 4 °C for 48 h. Labeling was visualized by the method described previously [24].

Results

An epitope tag composed of eight amino acids (FLAG marker peptide, Asp–Tyr–Lys–Asp–Asp–Asp–Lys) was fused upstream to the coding region of the wild-type and mutated SOD1 cDNA. Each of the cDNAs of the wild-type SOD1 and four mutant SOD1s linked to FALS (G37R, G85R, G93A, and S134N) was subcloned into two different expression vectors, pcDNA3 and pEF-BOS, and transfected into COS7 cells. After transfection and a 48-h culture, the cells were processed for Western blot analysis and immunocytochemistry.

The expression of wild-type and four FALS-linked mutant SOD1s in COS7 cells was confirmed by Western blot anlaysis of lysates using the anti-FLAG (M2) monoclonal antibody (Fig. 1). The molecular size of G85R was smaller than those of wild-type and the other mutants (Figs. 1A and B). Both wild-type and mutant SOD1s were expressed at much higher levels using pEF-BOS than pcDNA3 (Figs. 1A and B). The expression level of wild-type SOD1 in pEF-BOS was about 8.8 times as high as that in pcDNA3, and the expression levels of mutant SOD1s in pEF-BOS were 2.0 to 8.3 times as high as those in pcDNA3 by densitometry. Using pEF-BOS, the expression levels of mutant SOD1s were about 16–49% of the wild-type SOD1 by densitometry (Fig. 1A). On the other hand, such a marked decrease in the expression of mutant SOD1s was not apparent when pcDNA3 was employed (Fig. 1B). Using pEF-BOS, although the wild-type SOD1 was almost completely recovered in the cytosol fraction, a small amount of the mutant SOD1 protein remained in the pellet (Fig. 1C). Mutant G93A SOD1 protein in the pellet was about 30% of the total protein by densitometry (Fig. 1D).

Using pcDNA3, wild-type and mutant SOD1s were expressed and distributed diffusely throughout the cytoplasm of the transfected COS7 cells (Fig. 2). There was no obvious difference in the distribution pattern among them. Using pEF-BOS, the wild-type SOD1 also located diffusely in the cytoplasm, a result similar to that with the use of pcDNA3 (Fig. 2). On the other hand, mutant SOD1 expression using pEF-BOS produced

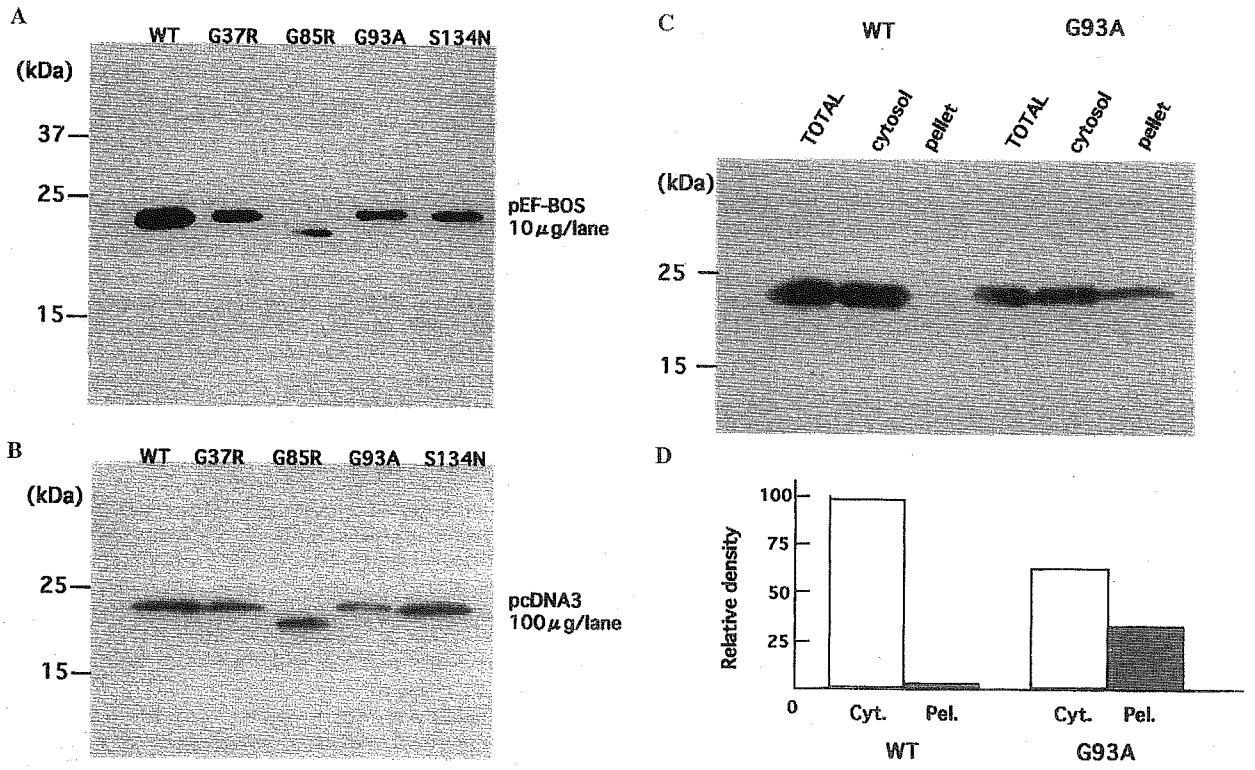

Fig. 1. Immunoblot analysis of wild-type (WT) and mutant (G37R, G85R, G93A, and S134N) SOD1s in total cell lysates derived from COS7 cells 48 h after transfection with SOD1 cDNA in pEF-BOS (A) or pcDNA3 (B). Ten mg (A) or 100 μg (B) of protein is applied to each lane. WT SOD1 expressed in COS7 cells is almost completely recovered in the cytosol fraction, whereas ~30% of mutant (G93A) SOD1 is in the pellet (C, D). Cyt, cytosol fraction; Pel, pellet. Expressed SOD1 is detected by anti-FLAG antibody (A–C). (D) Densitometry analysis (the density of wild-type SOD1 in cytosol fraction = 100%).

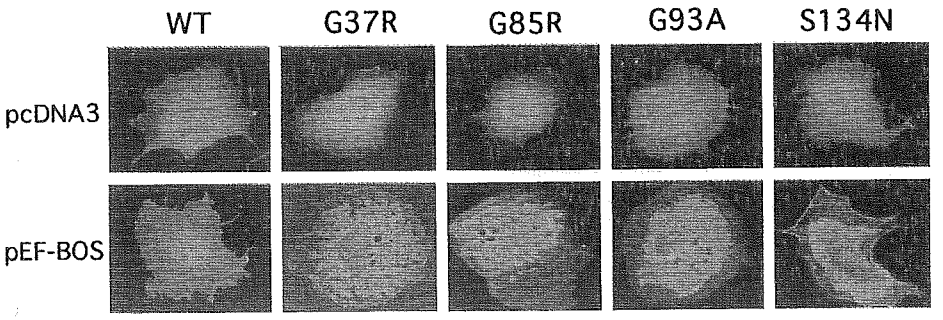

Fig. 2. Fluorescent microscopy of COS7 cells expressing wild-type (WT) and mutant (G37R, G85R, G93A, and S134N) SOD1s using pcDNA3 (upper panels) or pEF-BOS (lower panels). WT and mutant SOD1s expressed by pcDNA3 show a diffuse distribution in the cytoplasm. WT SOD1 expressed by pEF-BOS also shows a diffuse distribution, whereas mutant SOD1s by pEF-BOS produce an aggregate formation in the perinuclear area of the cytoplasm. Expressed SOD1 is detected by an anti-FLAG antibody.

aggregates of the mutant protein in the perinuclear region of the cytoplasm (Fig. 2). The cells containing these aggregates comprised 5–20% of the total transfected cells.

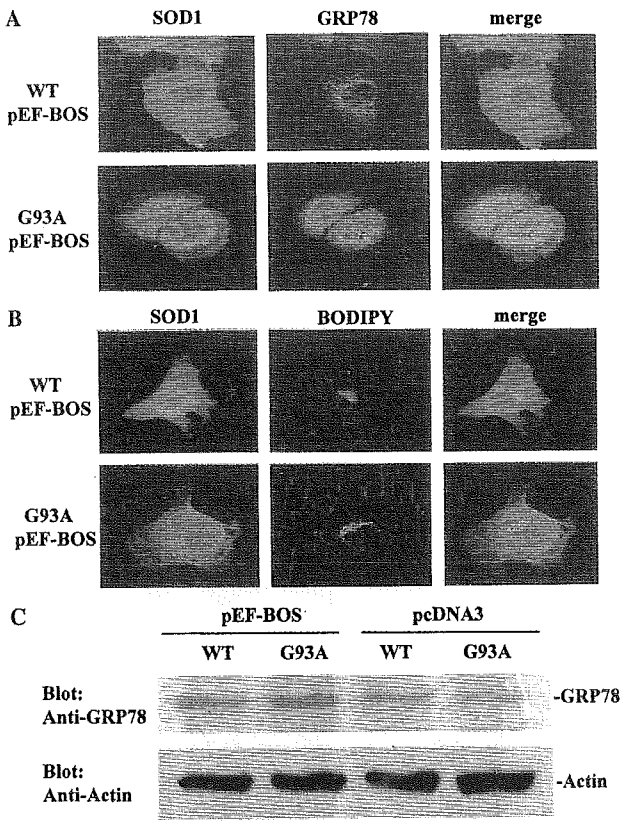

Fig. 3. COS7 cells expressing WT (upper panels) or mutant (G93A) SOD1 (lower panels) using pEF-BOS. (A) Double-staining with anti-FLAG (red) and anti-GRP78 (green) antibodies. Perinuclear aggregates of mutant SOD1 are colocalized with GRP78, an ER marker (lower panels). The overexpression of GRP78 is also observed in a mutant SOD1-expressing cell (middle in lower panels). (B) Double-labeling with anti-FLAG antibody (red) and BODIPY FL-C5 ceramide, a Golgi marker (green). (C) Immunoblot analysis showing that GRP78 expression is increased in COS7 cells transfected with a mutant (G93A) SOD1 cDNA in pEF-BOS.

The subcellular localization of the mutation-related perinuclear aggregates was then examined. COS7 cells expressing wild-type SOD1 or mutant SOD1s were double-stained with the anti-FLAG (M2) antibody and the ER markers (ER tracker and anti-GRP78/BiP antibody) or the Golgi marker (BODIPY-C5 ceramide) (Fig. 3). In the COS7 cells transfected with the wild-type SOD1 cDNA in pcDNA3 or pEF-BOS, both the ER (Fig. 3A) and Golgi apparatus (Fig. 3B) showed a normal morphology in the juxta-nuclear position. In the cells transfected with a mutant SOD1 cDNA in pEF-BOS, on the other hand, perinuclear aggregates of mutant SOD1 colocalized with the two ER markers (Fig. 3A), indicating accumulation of aggregated mutant SOD1 in or on the ER. A volume expansion of the ER in these cells was also observed. Western blot analysis confirmed an increase in the expression of GRP78/BiP in these cells (Fig. 3C). However, the aggregate of the mutant SOD1 was not colocalized with the Golgi marker (Fig. 3B), indicating that Golgi complex is not involved.

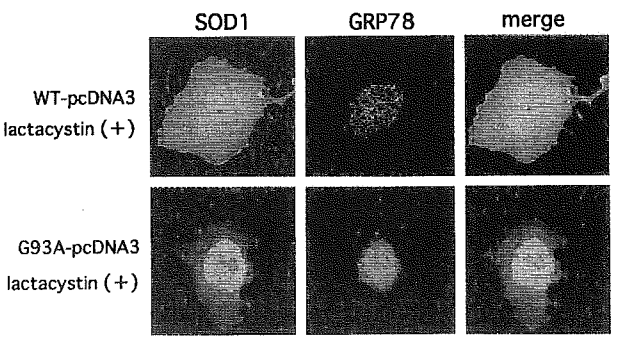

Fig. 4. COS7 cells expressing WT (upper panels) or mutant (G93A) SOD1 (lower panels) using pcDNA3 double-stained with anti-FLAG (red) and anti-GRP78 (green) antibodies. The exposure to lactacystin, a proteasome inhibitor, produces perinuclear aggregates of mutant SOD1, but not WT SOD1. Overexpression of GRP78 is also seen in a cell with aggregate formation of mutant SOD1 (middle in lower panels).

To examine the involvement of the proteasome function in the formation of perinuclear aggregates, a proteasome inhibitor, lactacystin, was used. When cells expressing wild-type or mutant SOD1s using pcDNA3 were exposed to 10 μM lactacystin for 24 h, perinuclear aggregates of SOD1 occurred in the cells expressing the mutant, but not the wild-type, SOD1 (Fig. 4). Perinuclear aggregates were colocalized with the ER markers and the ER was seen to be expanded (Fig. 4). These changes were almost identical to those of the mutant SOD1s expressed by pEF-BOS. This suggests that mutant SOD1s were degraded by proteasome and that the suppression of proteasome activity by lactacystin caused an accumulation of mutant SOD1 in association with the ER.

The influence of perinuclear aggregates of mutated SOD1 on the cytoskeleton and mitochondria was examined next. In the cells expressing wild-type SOD1 using pEF-BOS, actin stress fibers visualized by phalloidin-Alexa 568 were abundant in number and distributed to both the perinuclear and peripheral areas of the cytoplasm (Fig. 5A). In the cells expressing mutant SOD1s using pEF-BOS, actin stress fibers were obviously decreased in number, but their organization and distribution seemed unchanged (Fig. 5A). Microtubules detected by the anti-tubulin antibodies were observed to radiate to the periphery of the cytoplasm from the centrosome in the cells expressing wild-type SOD1 using pEF-BOS (Fig. 5B). In the cells expressing mutant SOD1s using pEF-BOS, however, the fiber formation of tubulin was disrupted and the location of tubulin was restricted to the perinuclear area of the cytoplasm (Fig. 5B). Mitochondria detected by the anti-SOD2 antibodies showed a normal morphology and distribution in the cytoplasm of cells expressing wild-type SOD1 using pEF-BOS (Fig. 5C). In cells expressing mutant SOD1 using pEF-BOS, however, mitochondria were confined to the perinuclear area of the cytoplasm and showed a

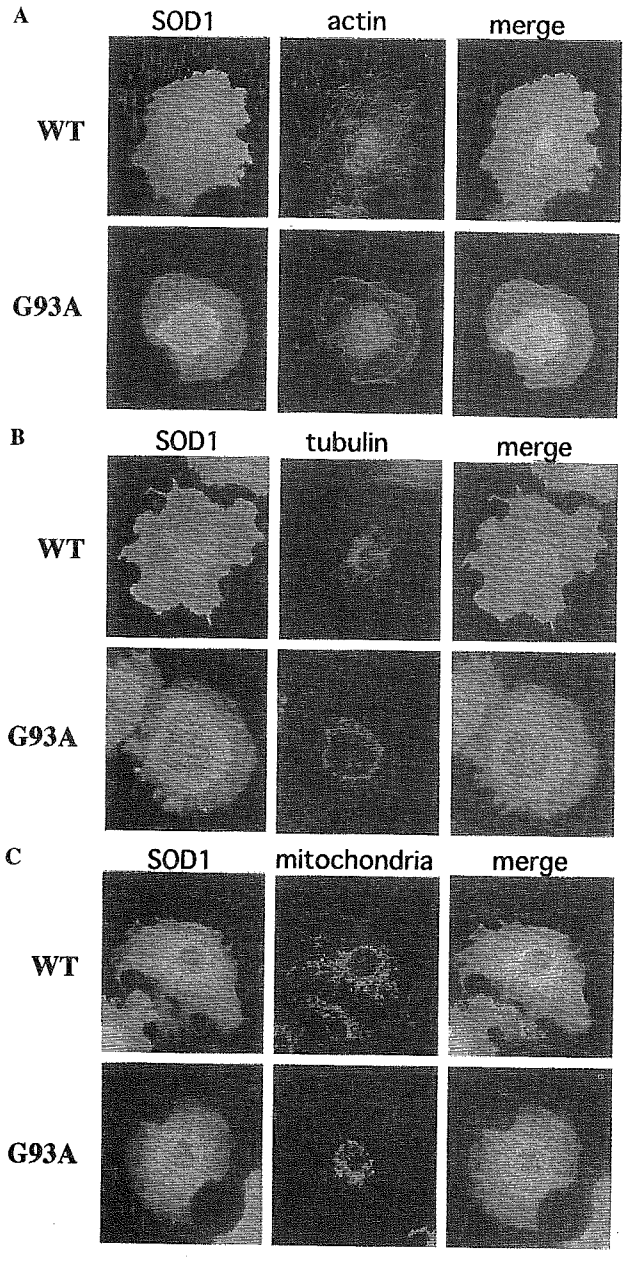

Fig. 5. COS7 cells expressing WT (upper panels) or mutant (G93A) SOD1 (lower panels) using pEF-BOS. (A) Double-staining with anti-FLAG antibody (red) and Alexa Fluor TM 568 phalloidin (green), an actin marker. Actin stress fibers are decreased in number, but their intracytoplasmic distribution seems unchanged in a cell with aggregate formation of mutant SOD1 (middle in lower panels). (B) Double-staining with anti-FLAG (red) and anti-tubulin (green) antibodies. Tubulin is restricted to the perinuclear area and does not show a fibrous appearance in a cell with aggregate formation of mutant SOD1 (middle in lower panels). (C) Double-staining with anti-FLAG (red) and anti-SOD2 (green) antibodies. SOD2, a marker of mitochondria, is restricted to the perinuclear area in a cell with aggregate formation of mutant SOD1 (middle in lower panels).

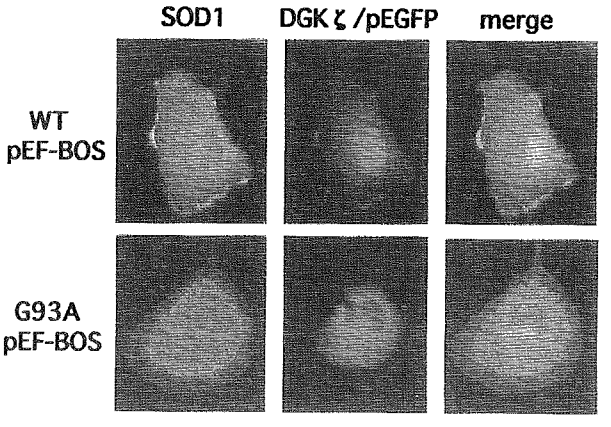

Fig. 6. COS7 cells co-transfected with WT (upper panels) or mutant (G93A) (lower panels) SOD1 (red) cDNA in pEF-BOS and diacylglycerol kinase ζ (DGK ζ) (green) cDNA in pEGFP-C2. Expressed DGK ζ, normally localized in the nucleus (middle in upper panels), does not reach the nucleus in a cell with aggregate formation of mutant SOD1 (middle in lower panels).

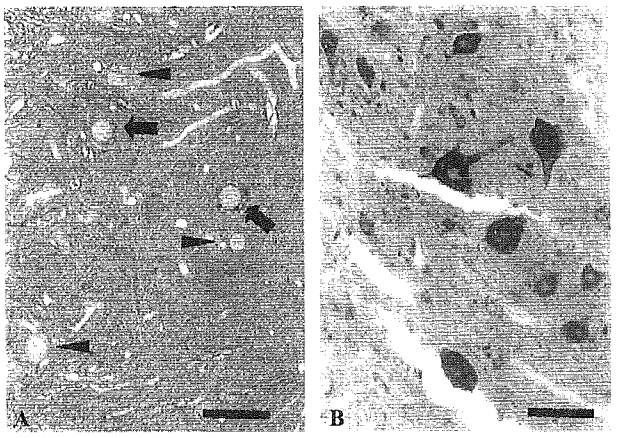

Fig. 7. Motor neurons of the spinal cord in non-transgenic (A) and transgenic mice with SOD1 mutation (L84V) (B), immunostained with anti-GRP78/BiP. Intense immunoreactivity is seen in virtually all motor neurons in a mouse with L84V mutation of the SOD1 transgene (B), although a few motor neurons (arrows) show a weak immunostaining in a non-transgenic mouse (A). The arrowheads indicate unstained motor neurons. Bar = 50 μm.

coarse appearance suggesting a morphology of mitochondrial swelling (Fig. 5C).

To examine the influence of aggregate formation on the localization of other proteins, a nuclear protein, diacylglycerol kinase ζ (DGK ζ) [23], was used. In co-transfected cells with wild-type SOD1 in pEF-BOS and rat DGK ζ in pEGFP, the expressed DGK ζ was localized in the nucleus (Fig. 6) as described previously [23]. In co-transfected cells with mutant SOD1s in pEF-BOS and DGK ζ in pEGFP, on the other hand, most DGK ζ remained in the cytoplasm and colocalized with the aggregates of mutant SOD1s, but did not reach the nucleus (Fig. 6).

For the investigation of ER changes in the mouse model of FALS, two lines of transgenic mice (L84V and H46R) and age-matched non-transgenic mice were used. These two transgenic mice showed an intense immunostaining of GRP78/BiP, an ER chaperone, in the cytoplasm of virtually all motor neurons of the spinal cord just before the onset of motor symptoms, whereas the non-transgenic mice showed a weak immunostaining in a few motor neurons (Fig. 7).

Discussion

The present study demonstrates that the FALS-linked mutation of SOD1 leads to aggregate formation in the cDNA-transfected COS7 cells in the condition that either drives gene expression at a high level (pEF-BOS) or suppresses the proteasome activity by lactacystin. The finding that FALS-linked mutant SOD1 was aggregated in transfected cultured cells has been reported by the previous studies [25,26]. Here we show for the first time that the pathological process is clearly dependent on the expression level of the mutants and the activity level of protein degradation. It should also be noted that the mutation-related aggregates are colocalized with the expanded ER. The results strongly suggest association of the aggregate with the ER.

The function of most proteins depends on the proper three-dimensional conformation of their mature, folded forms. Misfolding or unfolding of proteins after biosynthesis can be repaired through the quality-control system of the ER [27]. An accumulation of misfolded or unfolded proteins in the ER induces ER stress, in which three different mechanisms are known to be activated: transcriptional induction of ER-resident chaperones, translational attenuation of the misfolded or unfolded proteins, and their degradation through the ubiquitin-proteasome system [27]. In the present study, the decreased solubility of mutant SOD1 proteins in the cytosol (Fig. 1D) suggests a conformational change of the mutant proteins. This is in agreement with the report that insoluble, high-molecular-weight complexes of mutant SOD1 are detectable several months before the onset of the disease in a mouse model with a FALS-linked mutant SOD1 transgene [21]. Our observation revealed not only colocalization of the aggregated mutant proteins with the ER markers but also the up-regulation of GRP78/BiP expression in the transfected COS7 cells (transcriptional induction). In the high-expression system (pEF-BOS), on the other hand, the amount of mutant SOD1 proteins in the transfected COS7 cells was less than that in the wild-type SOD1, suggesting a translational attenuation or an increase in the degradation of the mutants. The inhibition of proteasome activity by lactacystin exposure produced an aggregation of mutant SOD1 in the lower-expression system (pcDNA3), indicating that the proteasome system is involved in the degradation of the mutant proteins. All these results are compatible with the quality-control system of the ER described above, demonstrating that the mutant SOD1s linked to FALS might induce ER stress in the transfected COS7 cells. In such cells, tubulin and mitochondria did not reach their proper intracellular locations, but were confined to the perinuclear region. The fluorescent images of tubulin and mitochondria were seen to be just surrounded by the aggregates (Figs. 5B and C), suggesting that outgrowth of tubulin from the centrosome was spatially blocked by the aggregates. The mitochondrial dislocation may be due to a restricted tubulin outgrowth, because this organelle is transported throughout the cytoplasm on microtubules, but not actin filament. A nuclear protein, DGK ζ, which was co-transfected with mutant SOD1 into COS7 cells, was also colocalized with the aggregates of the mutant associated with the ER. These data suggest that even non-mutated proteins suffer from ER dysfunction and are trapped in the

aggregates in an overexpression condition beyond a physiological condition. Considering that the very early change in transgenic mice with FALS-linked SOD1 mutation is an impairment of axonal transport [28], it seems that the FALS-linked mutant SOD1 also caused an impairment of the intracellular transport system in the transfected COS7 cells.

With regard to the subcellular localization of SOD1, the previous studies have reported that SOD1 is preferentially synthesized by free ribosomes in the in vitro experiments [29] and is localized mainly in the cytoplasm and the nucleus and partially in mitochondria [30–32]. In pathologic conditions such as hepatitis and cirrhosis, however, SOD1 has been shown to localize in the ER, vesicles, and Golgi complex in hepatocytes [33]. Little is known about the mechanism how SOD1 is transported from the cytoplasm to the membranous organelles, although it is reported that the mitochondrial accumulation of SOD1 is strongly influenced by the copper chaperone [34]. In the present study, although the aggregated mutant SOD1 was closely associated with the expanded ER, it remains unclear whether it is localized within the cistern of the ER or outside.

In human FALS with an SOD1 mutation, there are two major mysteries: motor neuron selectivity and adult onset. Although every cell has mutant SOD1 in FALS patients, the motor neurons seem to degenerate selectively. The answer to this mystery is that the functional integrity of motor neurons is critically dependent on vigorous intracellular transport, especially axonal transport, because a motor neuron has an enormously long axon (about 1 m in length). The dysfunction of intracellular transport, the degree of which does not have an apparent effect on the function or survival of non-motor neurons or non-nerve cells, may do great damage to motor neurons. The other mystery is the adult onset of the disease in spite of the presence of mutant SOD1 even in newborns. In the present study, a lower expression of the mutant SOD1 by the pcDNA3 vector did not produce any aggregation of the mutant protein or induce ER stress. However, the inhibition of proteasome activity by exposure to lactacystin produced an aggregation of the mutant protein and a dislocation of tubulin, mitochondria, and DGK ζ. The proteasome activity has been reported to decrease with aging in animals [35]. A decrease in proteasome activity paired with aging may allow the insoluble, high-molecular-weight complexes of mutant SOD1 to be accumulated beyond a non-compensable level in both patients and transgenic mice with a FALS-linked SOD1 mutation, resulting in the adult onset of the disease.

It has been shown that the knock-out of the SOD1 gene does not produce any neurological symptoms or pathologic changes in mice [7] and that the overexpression of wild-type SOD1 does not modulate the pathology in transgenic mice with the FALS-linked mutant SOD1 [15]. Thus, a decrease or increase in SOD1 activity, as well as the formation of peroxynitrite and subsequent tyrosine nitration of proteins, seems to be unrelated to the pathogenesis of FALS with an SOD1 mutation. Recently, a conformational change of a certain protein and subsequent ER stress have been shown to be an important step in the pathogenesis of neurodegenerative diseases, such as Alzheimer's disease, Parkinson's disease, and Creutzfeldt-Jakob disease [18–20,36,37]. The present study demonstrates that the FALS-linked mutant SOD1 caused ER stress and a possible disruption of the intracellular transport in the transfected COS7 cells, which may explain how the mutant SOD1 gains a toxic function. In transgenic mice with SOD1 mutation, the overexpression of GRP78/BiP, an ER-resident chaperone, was also observed in motor neurons of the spinal cord before onset of the disease. These data suggest that ER stress is involved in the pathogenesis of FALS with an SOD1 mutation. It seems that human FALS with an SOD1 mutation is also a conformational disease of the SOD1 molecule.

Acknowledgments

We are grateful to Professor Kimishige Ishizaka, La Jolla Institute for Allergy & Immunology, for critically reviewing the manuscript. This work was supported by grants from the Ministry of Education, Science, Sports and Culture of Japan, and from the Ministry of Health and Welfare of Japan.

References

[1] D.R. Rosen, Mutations in Cu/Zn superoxide dismutase gene are associated with familial amyotrophic lateral sclerosis, Nature 364 (1993) 362.

[2] H.X. Deng, A. Hentati, J.A. Tainer, Z. Iqbal, A. Cayabyab, W.Y. Hung, E.D. Getzoff, P. Hu, B. Herzfeldt, R.P. Roos, Amyotrophic lateral sclerosis and structural defects in Cu, Zn-superoxide dismutase, Science 261 (1993) 1047–1051.

[3] C.E. Shaw, Z.E. Enayat, B.A. Chioza, A. Al Chalabi, A. Radunovic, J.F. Powell, P.N. Leigh, Mutations in all five exons of SOD-1 may cause ALS, Ann. Neurol. 43 (1998) 390–394.

[4] M. Aoki, M. Ogasawara, Y. Matsubara, K. Narisawa, S. Nakamura, Y. Itoyama, K. Abe, Mild ALS in Japan associated with novel SOD mutation, Nat. Genet. 5 (1993) 323–324.

[5] R. Orrell, J. de Belleroche, S. Marklund, F. Bowe, R. Hallewell, A novel SOD mutant and ALS, Nature 374 (1995) 504–505.

[6] A.C. Bowling, J.B. Schulz, R.H. Brown Jr., M.F. Beal, Superoxide dismutase activity, oxidative damage, and mitochondrial energy metabolism in familial and sporadic amyotrophic lateral sclerosis, J. Neurochem. 61 (1993) 2322–2325.

[7] A.G. Reaume, J.L. Elliott, E.K. Hoffman, N.W. Kowall, R.J. Ferrante, D.F. Siwek, H.M. Wilcox, D.G. Flood, M.F. Beal, R.H. Brown Jr., R.W. Scott, W.D. Snider, Motor neurons in Cu/Zn superoxide dismutase-deficient mice develop normally but exhibit enhanced cell death after axonal injury, Nat. Genet. 13 (1996) 43–47.

[8] M.E. Gurney, H. Pu, A.Y. Chiu, M.C. Dal Canto, C.Y. Polchow, D.D. Alexander, J. Caliendo, A. Hentati, Y.W. Kwon, H.X.

Deng, Motor neuron degeneration in mice that express a human Cu, Zn- superoxide dismutase mutation, Science 264 (1994) 1772–1775.
[9] P.C. Wong, C.A. Pardo, D.R. Borchelt, M.K. Lee, N.G. Copeland, N.A. Jenkins, S.S. Sisodia, D.W. Cleveland, D.L. Price, An adverse property of a familial ALS-linked SOD1 mutation causes motor neuron disease characterized by vacuolar degeneration of mitochondria, Neuron 14 (1995) 1105–1116.
[10] M.E. Ripps, G.W. Huntley, P.R. Hof, J.H. Morrison, J.W. Gordon, Transgenic mice expressing an altered murine superoxide dismutase gene provide an animal model of amyotrophic lateral sclerosis, Proc. Natl. Acad. Sci. USA 92 (1995) 689–693.
[11] L.I. Bruijn, M.W. Becher, M.K. Lee, K.L. Anderson, N.A. Jenkins, N.G. Copeland, S.S. Sisodia, J.D. Rothstein, D.R. Borchelt, D.L. Price, D.W. Cleveland, ALS-linked SOD1 mutant G85R mediates damage to astrocytes and promotes rapidly progressive disease with SOD1-containing inclusions, Neuron 18 (1997) 327–338.
[12] T. Siddique, D. Nijhawan, A. Hentati, Molecular genetic basis of familial ALS, Neurology 47 (1996) S27–S34.
[13] D.R. Borchelt, M.K. Lee, H.S. Slunt, M. Guarnieri, Z.S. Xu, P.C. Wong, R.H. Brown Jr., D.L. Price, S.S. Sisodia, D.W. Cleveland, Superoxide dismutase 1 with mutations linked to familial amyotrophic lateral sclerosis possesses significant activity, Proc. Natl. Acad. Sci. USA 91 (1994) 8292–8296.
[14] D.W. Cleveland, N. Laing, P.V. Hurse, R.H. Brown Jr., Toxic mutants in Charcot's sclerosis, Nature 378 (1995) 342–343.
[15] L.I. Bruijn, M.K. Houseweart, S. Kato, K.L. Anderson, S.D. Anderson, E. Ohama, A.G. Reaume, R.W. Scott, D.W. Cleveland, Aggregation and motor neuron toxicity of an ALS-linked SOD1 mutant independent from wild-type SOD1, Science 281 (1998) 1851–1854.
[16] J.S. Beckman, M. Carson, C.D. Smith, W.H. Koppenol, ALS, SOD, and peroxynitrite, Nature 364 (1993) 584.
[17] M. Wiedau-Pazos, J.J. Goto, S. Rabizadeh, E.B. Gralla, J.A. Roe, M.K. Lee, J.S. Valentine, D.E. Bredesen, Altered reactivity of superoxide dismutase in familial amyotrophic lateral sclerosis, Science 271 (1996) 515–518.
[18] R.J. Ellis, T.J.T. Pinheiro, Danger-misfolding proteins, Nature 416 (2002) 483–484.
[19] M. Bucciantini, E. Giannoni, F. Chiti, F. Baroni, L. Formigli, J. Zurdo, N. Taddei, G. Ramponi, C.M. Dobson, M. Stefani, Inherent toxicity of aggregates implies a common mechanism for protein misfolding diseases, Nature 416 (2002) 507–511.
[20] D.M. Walsh, I. Klyubin, J.V. Fadeeva, W.K. Cullen, R. Anwyl, M.S. Wolfe, M.J. Rowan, D.J. Selkoe, Naturally secreted oligomers of amyloid beta protein potently inhibit hippocampal long-term potentiation in vivo, Nature 416 (2002) 535–539.
[21] J.A. Johnston, M.J. Dalton, M.E. Gurney, R.R. Kopito, Formation of high-molecular weight complexes of mutant Cu, Zn-superoxide dismutase in a mouse model for familial amyotrophic lateral, Proc. Natl. Acad. Sci. USA 97 (2000) 12571–12576.
[22] S. Mizushima, S. Nagata, pEF-BOS, a powerful mammalian expression vector, Nucleic Acids Res. 18 (1990) 5322.
[23] K. Goto, H. Kondo, A 104-kDa diacylglycerol kinase containing ankyrin-like repeats localizes in the cell nucleus, Proc. Natl. Acad. Sci. USA 93 (1996) 11196–11201.
[24] T. Kato, K. Kurita, T. Seino, T. Kadoya, H. Horie, M. Wada, T. Kawanami, M. Daimon, A. Hirano, Galectin-1 is a component of neurofilamentous lesions in sporadic and familial amyotrophic lateral sclerosis, Biochem. Biophys. Res. Commun. 282 (2001) 166–172.
[25] H.D. Durham, J. Roy, L. Dong, D.A. Figlewicz, Aggregation of mutant Cu/Zn superoxide dismutase proteins in a culture model of ALS, J. Neuropathol. Exp. Neurol. 56 (1997) 523–530.
[26] T. Koide, S. Igarashi, K. Kikugawa, R. Nakano, T. Inuzuka, M. Yamada, H. Takahashi, S. Tsuji, Formation of granular cytoplasmic aggregates in COS7 cells expressing mutant Cu/Zn superoxide dismutase associated with familial amyotrophic lateral sclerosis, Neurosci. Lett. 257 (1998) 29–32.
[27] K. Mori, Tripartite management of unfolded proteins in the endoplasmic reticulum, Cell 101 (2000) 451–454.
[28] T.L. Williamson, D.W. Cleveland, Slowing of axonal transport is a very early event in the toxicity of ALS-linked SOD1 mutants to motor neurons, Nat. Neurosci. 2 (1999) 50–56.
[29] K. Hirano, M. Fukuta, T. Adachi, K. Hayashi, M. Sugiura, Y. Mori, K. Toyoshi, In vitro synthesis of superoxide dismutases of rat liver, Biochem. Biophys. Res. Commun. 129 (1985) 89–94.
[30] L.Y. Chang, J.W. Slot, H.J. Geuze, J.D. Crapo, Molecular immunocytochemistry of the Cu, Zn-superoxide dismutase in rat hepatocytes, J. Cell Biol. 107 (1988) 2169–2179.
[31] J. Nishiyama, Immunoelectron microscopic localization of copper–zinc superoxide dismutase in human gastric mucosa, Acta Histochem. Cytochem. 29 (2002) 215–220.
[32] A. Okado-Matsumoto, I. Fridovich, Subcellular distribution of superoxide dismutases (SOD) in rat liver: Cu, Zn-SOD in mitochondria, J. Biol. Chem. 276 (2001) 38388–38393.
[33] T. Saito, H. Shinzawa, H. Togashi, H. Wakabayashi, K. Ukai, T. Takahashi, M. Ishikawa, M. Dobashi, Y. Imai, Ultrastructural localization of Cu, Zn-SOD in hepatocytes of patients with various liver diseases, Histol. Histopath. 4 (1989) 1–6.
[34] L.A. Sturtz, K. Diekert, L.T. Jensen, R. Lill, V.C. Culotta, A fraction of yeast Cu, Zn-superoxide dismutase and its metallochaperone, CCS, localize to the intermembrane space of mitochondria. A physiological role for SOD1 in guarding against mitochondrial oxidative damage, J. Biol. Chem. 276 (2001) 38084–38089.
[35] J.N. Keller, F.F. Huang, W.R. Markesbery, Decreased levels of proteasome activity and proteasome expression in aging spinal cord, Neuroscience 98 (2000) 149–156.
[36] T. Jin, Y. Gu, G. Zanusso, M. Sy, A. Kumar, M. Cohen, P. Gambetti, N. Singh, The chaperone protein BiP binds to a mutant prion protein and mediates its degradation by the proteasome, J. Biol. Chem. 275 (2000) 38699–38704.
[37] Y. Imai, M. Soda, H. Inoue, N. Hattori, Y. Mizuno, R. Takahashi, An unfolded putative transmembrane polypeptide, which can lead to endoplasmic reticulum stress, is a substrate of Parkin, Cell 105 (2001) 891–902.

Glycation proceeds faster in mutated Cu, Zn-superoxide dismutases related to familial amyotrophic lateral sclerosis[1]

RINA TAKAMIYA, MOTOKO TAKAHASHI, THEINGI MYINT, YONG SEEK PARK, NOBUKO MIYAZAWA, TAKESHI ENDO, NORIKO FUJIWARA, HARUHIKO SAKIYAMA, YOSHIKO MISONOU, YASUHIDE MIYAMOTO, JUNICHI FUJII,* AND NAOYUKI TANIGUCHI[2]

Department of Biochemistry, Osaka University Medical School, Suita, Osaka 565-0871, Japan; and *Department of Biochemistry, Yamagata University School of Medicine, Yamagata 990-9585, Japan

SPECIFIC AIMS

Although nearly 100 types of different mutations in Cu, Zn-superoxide (Cu, Zn-SOD) have been found in familial ALS (FALS) patients, the mechanisms by which those mutants of Cu, Zn-SOD lead to neurodegenerative disorder have so far not been fully elucidated. To elucidate the pathological role of mutated Cu, Zn-SOD in FALS, the susceptibility of mutated Cu, Zn-SODs to glycation was examined.

PRINCIPAL FINDINGS

1. Mutated Cu, Zn-SODs are susceptible to glycation

Wild-type (WT) and three mutated Cu, Zn-SODs—G37R, G93A, and I113T—were produced in the baculovirus/Sf21 insect cell system. To examine the susceptibility of mutated Cu, Zn-SODs to glycation, purified WT and mutated Cu, Zn-SODs were incubated with 100 mM glucose at 37°C for 14 days, and the glycated proteins were quantified by Western blot using the anti-hexitol lysine antibody, which reacts with the reduced Amadori product, an early glycation product. The mutated enzymes (G37R, G93A, I113T) were more highly glycated than in the WT enzyme. Moreover, glycated forms were detected in the mutants even before incubation with glucose, suggesting that mutated Cu, Zn-SODs were glycated during the 4 days incubation with ~4 mM glucose present in the culture medium. We next separated glycated and nonglycated Cu, Zn-SODs using a boronate affinity column and the nonglycated fractions were incubated with various concentrations of glucose. **Figure 1***A* shows data on the dose-dependent glycation of nonglycated fractions of Cu, Zn-SODs, as quantified by Western blot using the anti-hexitol lysine antibody. Before incubating with glucose, it was confirmed that neither the WT nor the mutated Cu, Zn-SODs (G37R, G93A) were glycated. After incubation with 1 or 10 mM glucose at 37°C for 7 days, the glycation reaction was dose dependent and the mutated Cu, Zn-SODs (G37R, G93A) were more susceptible to glycation than the WT. Figure 2 indicates that glycation occurred in a time-dependent manner and that G93A was more susceptible to glycation than the WT.

2. Mutated Cu, Zn-SODs are susceptible to fructation

Since fructose is a more potent glycating agent than glucose, we also examined the effects of fructose. After separation of glycated and nonglycated Cu, Zn-SODs using a boronate affinity column, the nonglycated proteins were incubated with 1 or 10 mM fructose for 3 days. G93A and G37R were more susceptible to fructation than the WT enzyme, and fructation occurred in dose-dependent manner.

3. Mutated Cu, Zn-SOD (G93A) produces more hydrogen peroxide from glycation and fructation

As we previously reported, a site-specific fragmentation of Cu, Zn-SOD is caused by ROS formed from the glycation reaction. To identify the radical species produced during glycation, ESR spectra were measured using DMPO as a trapping agent. When 1 mg/mL of WT or mutated Cu, Zn-SODs were incubated with 100 mM glucose at 37°C for 7 days, no signal was observed. We next examined the production of hydrogen peroxide, since superoxide anion is thought to be generated from glycation reaction, then the hydrogen peroxide could be formed by a dismutase activity of Cu, Zn-SOD. As shown in **Fig. 2***A*, when G93A and WT Cu, Zn-SODs were incubated with 100 mM glucose or 1 mM fructose, hydrogen peroxide was produced in time-dependent manner; the level of hydrogen peroxide produced from G93A was almost twice that of the WT. In this system, ROS produced by glucose autoxidation was included;

---

[1]To read the full text of this article, go to http://www.fasebj.org/cgi/doi/10.1096/fj.02-0768fje; to cite this article, use *FASEB J.* (March 5, 2003) 10.1096/fj.02-0768fje

[2]Correspondence: Department of Biochemistry, Department of Biochemistry, Osaka University Medical School, 2-2 Yamadaoka, Suita, Osaka 565-0871, Japan. E-mail: proftani@biochem.med.osaka-u.ac.jp

0892-6638/03/0017-0938 © FASEB

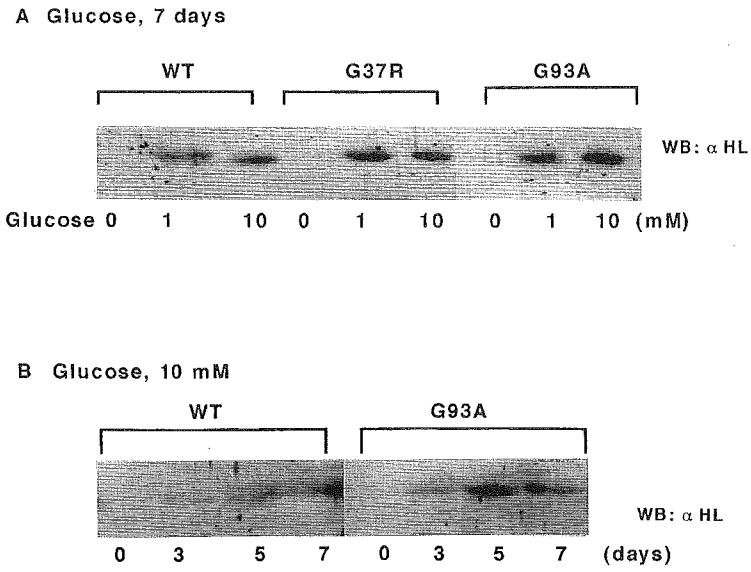

Figure 1. Dose- and time-dependent glycation of mutated Cu, Zn-SODs. After separating glycated and nonglycated Cu, Zn-SOD by boronate affinity column, nonglycated fractions were incubated with glucose. Glycated proteins were detected by Western blot using an anti-hexitol lysine antibody. *A)* Dose-dependent glycation of wild-type (WT) and mutated Cu, Zn-SODs (G37R, G93A). Proteins (0.5 mg/mL) were incubated with the indicated concentration of glucose at 37°C for 7 days. *B)* Time-dependent glycation of G93A and WT. Proteins (0.5 mg/mL) were incubated with 10 mM glucose. Each lane contains 0.5 μg of protein.

therefore, we next excluded free glucose or fructose by dialysis against 50 mM potassium phosphate buffer (pH 7.4). After dialysis, these samples were further incubated at 37°C and the extent of hydrogen peroxide production was measured. As seen in Fig. 2*B*, glycated and fructated G93A produced more hydrogen peroxide than the glycated and fructated WT, respectively.

CONCLUSIONS AND SIGNIFICANCE

Glycation of FALS-related mutants of Cu, Zn-SOD was examined. When the purified proteins were incubated with glucose, all the mutated Cu, Zn-SODs were found to be more susceptible to glycation than the WT. The mutated Cu, Zn-SODs were also more susceptible to fructation than the WT. When glycated Cu, Zn-SOD were incubated, hydrogen peroxide was produced, and the mutated Cu, Zn-SODs produced high levels in proportion to the extent of glycation. Production of hydrogen peroxide was also observed when fructated proteins were incubated; again, the mutants produced more hydrogen peroxide than the WT. It has been reported that Lewy body-like hyaline inclusions characteristically found in FALS patients are immunopositive both Cu, Zn-SOD and AGEs such as CML, pyrraline and pentosidine. From our data using purified Cu, Zn-SOD, the origin of these immunopositive lesions could be Cu, Zn-SOD itself, and it is likely that the glycation of mutated Cu, Zn-SODs is accelerated in vivo as well.

The primary characteristic of ALS is the selective degeneration of motor neurons, initiated in mid-adulthood. Since many different types of mutations in Cu, Zn-SOD have been observed in FALS, certain common characteristics of these mutants should explain the pathogenesis of the disease. Glycation proceeds through the formation of a Schiff base between reducing sugars and amine groups of lysine residues and a subsequent rearrangement to yield Amadori products, and finally produce AGEs, which have been shown to accumulate during aging. Glycation has been implicated in the chronic complications of diabetes mellitus and has been suggested to play an important role in the pathogenesis of neurodegenerative diseases. In this study, we hypothesize that the susceptibility of mutated Cu, Zn-SODs to glycation is a factor in the pathogenesis of FALS. An increased glycation has also been reported in sporadic ALS; Amadori products are present in axonal spheroids in the anterior horn of the spinal cord. The target protein of glycation in sporadic ALS is not known, but it is possible that some type of ROS produced during glycation is involved in the pathogenesis of sporadic ALS as well.

We previously reported that mutant enzymes form aggregates at a higher rate when incubated with copper ion and aggregates of mutant enzymes retain their enzymatic activity. Although glycation decreases the enzymatic activity of Cu, Zn-SOD, some activity should remain, and accelerated aggregation might play an important role in the microenvironment. Therefore, hydrogen peroxide could be produced by the aggregated forms of glycated Cu, Zn-SOD. We and other groups have also reported that the copper binding affinities were decreased in mutated Cu, Zn-SOD. This could be due to the instability of the mutated proteins, but it also could be due to glycation: we previously indicated that glycation causes the fragmentation of Cu, Zn-SOD.

These collective findings suggest that the glycation of mutated Cu, Zn-SODs can *1)* produce superoxide anion, and *2)* hydrogen peroxide is formed by the enzymatic activity of the aggregates, then *3)* hydroxyl radicals can be formed via the Fenton reaction involving the free copper ion released from the mutated Cu, Zn-SOD. In this study, hydroxyl radicals were not observed, but we assume that detection of this radical is dependent on the scale of the experiment; in the case of this study, the amount of free copper might not have

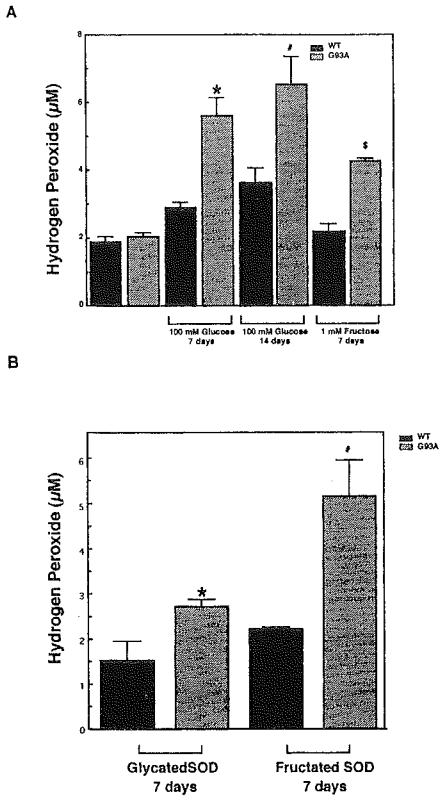

Figure 2. The production of hydrogen peroxide by incubation of wild-type and G93A Cu, Zn-SOD with glucose or fructose. *A)* 0.5 mg/mL WT or G93A was incubated with 100 mM glucose or 1 mM fructose for 7–14 days and hydrogen peroxide was measured. $^{*}P < 0.05$ compared with WT incubated with 100 mM glucose for 7 days. $\#P < 0.05$ compared with WT incubated with 100 mM glucose for 14 days. $^{\$}P < 0.05$ compared with WT incubated with 1 mM fructose for 7 days. *B)* After 0.5 mg/mL WT or G93A was incubated with 100 mM glucose or 1 mM fructose for 7 days, the samples were dialyzed against 50 mM potassium phosphate buffer (pH 7.4) to remove free glucose and fructose. The dialyzed Cu, Zn-SODs were incubated at 37°C for an additional 7 days. Data indicate mean ± SD of 3–4 separate experiments in each group. $^{*}P < 0.05$ compared with WT incubated with 100 mM glucose for 7 days. $\#P < 0.05$ compared with WT incubated with 1 mM fructose for 7 days.

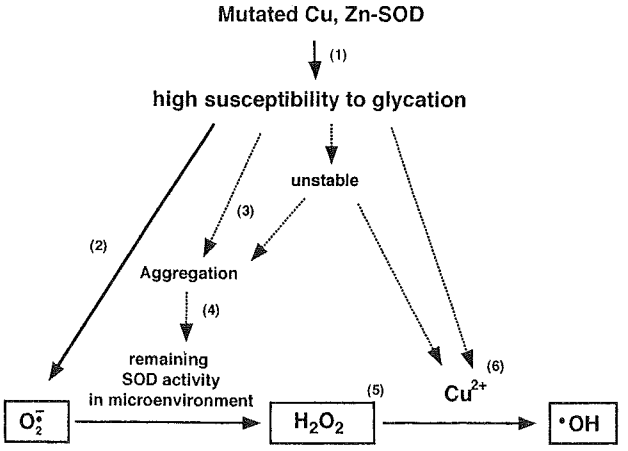

Figure 3. Schematic diagram illustrating the pathogenesis of FALS based on the susceptibility of mutated Cu, Zn-SOD to glycation. *1)* Mutated Cu, Zn-SODs are highly susceptible to glycation (Fig. 1). *2)* Superoxide anion is generated from the glycation reaction. *3)* The mutated Cu, Zn-SODs form aggregates at a higher rate. *4)* The aggregates of Cu, Zn-SODs retain their enzymatic activity. *5)* The mutated Cu, Zn-SOD produced higher levels of hydrogen peroxide by glycation than wild-type (Fig. 2). *6)* Copper binding affinities were decreased in mutated Cu, Zn-SOD.

been sufficient to accomplish this. Both hydrogen peroxide and hydroxyl radical are toxic to neuronal cells; thus, it is possible that the increased level of glycation of the mutated Cu, Zn-SOD (which requires a long time) induces toxic oxidative stress especially in the anterior horn of the spinal cord, which contains high levels of Cu, Zn-SOD. It is also possible that 3-deoxyglucosone, methylglyoxal, or AGEs produced from glycated Cu, Zn-SOD directly affect neuronal cell death, as has been suggested by other groups.

The mechanisms by which the mutation of Cu, Zn-SOD affects glycation are currently under investigation. Since it has been observed from many aspects that mutation of Cu, Zn-SODs leads to instability of the protein, it is possible that the exposure status or electronic environment of the lysine residues is altered in the case of mutants. Abnormal glucose tolerance has been reported in ~40% of ALS patients. Crystallographic studies are now under way, and we expect that structural information will provide us with clues for elucidating the mechanism whereby susceptibility to glycation is commonly observed in mutated Cu, Zn-SODs. FJ

ELSEVIER

Clinica Chimica Acta 327 (2003) 1–23

www.elsevier.com/locate/clinchim

Review

Hepatocyte growth factor: from diagnosis to clinical applications

Hiroshi Funakoshi, Toshikazu Nakamura*

Division of Molecular Regenerative Medicine, Course of Advanced Medicine, Osaka University Graduate School of Medicine, B-7 Osaka 565-0871, Japan

Received 10 May 2002; received in revised form 5 August 2002; accepted 19 August 2002

Abstract

Hepatocyte growth factor (HGF), initially identified and molecularly cloned as a potent mitogen of primary cultured hepatocytes, has multiple activities in a variety of tissues during the course of development and also in various disease states. HGF plays key roles in the attenuation of disease progression as an intrinsic repair factor. It is also evident that HGF levels are regulated under different conditions, for example, during the course of pregnancy, aging, and disease. This review focuses on the levels of HGF in normal and pathophysiological situations and examines the relationships between HGF levels and disease, disease stage, and disease prognosis. The clinical potential of HGF as a treatment for subjects with various diseases is also given attention.

Keywords: HGF; c-Met; Serum level; Tissue level; Disease; Gene therapy

1. Introduction

Numerous growth factors are regulated in a concerted fashion to maintain homeostasis, not only in healthy individuals responding to their surroundings, but also in subjects with diseases. Therefore, an understanding of the regulation and potential clinical applications of growth factors is of great importance.

Hepatocyte growth factor (HGF) was first identified in 1984 [1,2] and 1985 [3] and purified as a potent mitogen of primary cultured hepatocytes [4–6]. Molecular cloning revealed that it is a heterodimeric molecule composed of a 69-kDa α-chain and a 34-kDa β-chain. The α-chain contains an N-terminal hairpin domain and subsequent four-kringle domains, and the β-chain contains a serine protease-like domain with no enzymatic activity [7–9]. A fibroblast-derived epithelial cell motility factor, termed scatter factor, was identified in 1985 [10] and purified in 1989 [11]. Subsequent characterization revealed scatter factor to be identical to HGF [12–14]. HGF is synthesized and secreted as a biologically inactive

Abbreviations: AD, Alzheimer's disease; ChAT, choline acetyltransferase; CH, chronic hepatitis; CK, creatinine phosphokinase; CRP, C-reactive protein; DMN, dimethylnitrosamine; CsA, Cyclosporin A; CSF, cerebrospinal fluid; HCC, hepatocellular carcinoma; HGF, hepatocyte growth factor; HGF A, HGF activator; HVJ, hemagglutinating virus of Japan; LC, liver cirrhosis; OA, osteoarthritis; PAOD, peripheral arterial occlusive disease; RA, rheumatoid arthritis; TGF-β, transforming growth factor-β; TIF, tubulointerstitial fibrosis; TIL, tubulointerstitial lesion; uPA, urokinase-type plasminogen activator.

* Corresponding author. Tel.: +81-6-6879-3783; fax: +81-6-6879-3789.

E-mail address: nakamura@onbich.med.osaka-u.ac.jp (T. Nakamura).

0009-8981/02/$ - see front matter © 2002 Elsevier Science B.V. All rights reserved.
PII: S0009-8981(02)00302-9

single-chain precursor form, and further processing by serine proteases into the two-chain form is coupled to its activation (Fig. 1). Serine proteases responsible for the activation of HGF include HGF activator or HGF-converting enzyme and urokinase-type plasminogen activator (uPA) [15–18]. The receptor for HGF was identified as a c-met proto-oncogene product [19–21]. The c-Met receptor is composed of a 50-kDa α-chain and 145-kDa β-chain. The α-chain is exposed extracellularly, while the β-chain is a transmembrane subunit containing an intracellular tyrosine kinase domain. Binding of HGF to the c-Met receptor induces activation of tyrosine kinase, an event that results in subsequent phosphorylation of C-terminally clustered tyrosine residues (Fig. 1) [22]. Phosphorylation of these tyrosine residues recruits intracellular signaling molecules containing the src homology (SH) domain, including Gab-1, phospholipase c-γ (PLC-γ), Ras-GTPase activating protein (Ras-GAP), phosphatidylinositol 4,5-bisphosphate 3-kinase (PI-3 kinase), c-Src, Shp-2, Crk, and Grb-2. A potential contribution of Bag-1 and STAT3 for HGF signaling was also reported [23,24]. Although HGF was initially identified as a potent mitogen for hepatocytes, considerable evidence indicates that intracellular signaling pathways driven by HGF-c-Met receptor coupling lead to

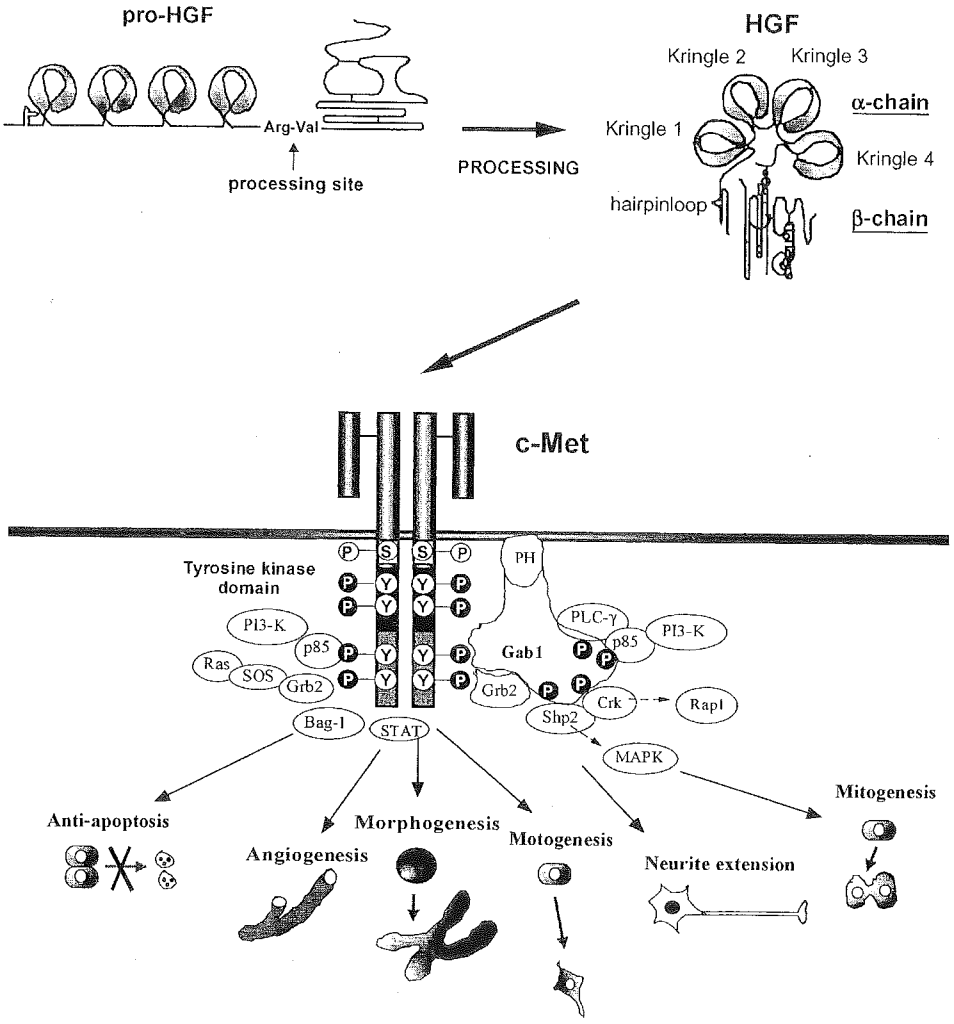

Fig. 1. Schematic structure of mature HGF processed from proHGF, and biological activities of mature HGF mediated by intracellular signals of the c-Met/HGF receptor.

multiple biological responses in a variety of cells, including mitogenic, motogenic (enhancement of cell motility), morphogenic, neurite extension and anti-apoptotic activities.

The essential role for HGF and the c-Met receptor in mammalian development was defined by the disruption of *HGF* or the *c-met* gene in mice; these mice died during development (embryonic days 13–15) as organogenesis of the placenta and liver was impaired. HGF is also involved in the formation of the kidney, lung, mammary gland, teeth, muscle, and neuronal tissues [25–31], and the organotypic role of HGF in the liver has been well defined [25].

In addition, HGF has an organotrophic role in the regeneration and protection of various organs, including the liver, lung, stomach, pancreas, heart, brain, and kidney [32–38]. As correlated with the role of HGF in such diseases, HGF levels are regulated in serum, bronchoalveolar lavage, cerebrospinal and synovial fluids, and/or tissues. In this review, we focus on the relationships between HGF levels and normo-physiological alterations or disease states and the clinical potential of HGF to treat individuals with diseases.

2. Hemodynamics of HGF

An understanding of the hemodynamics of HGF is essential to estimate the clinical relevance of an alteration of serum HGF levels. An injection study revealed that the percentage of ^{125}I-labeled HGF in the peripheral blood was 92.3% at 3 min, 86.5% at 30 min, 80.4% at 60 min, 69.4% at 120 min after the injection, and that ^{125}I-labeled HGF diffuses into the liver, adrenal gland, spleen, kidney, lung, stomach, and intestine within 3 min after intravenous injection of HGF, but does not diffuse into the heart or brain [39–43]. The clearance rate of ^{125}I-labeled HGF is about 70% in the liver and less than 10% in the kidney. Two mechanisms of HGF clearance have been hypothesized: one is internalization of HGF with c-Met and the other is trapping by binding molecules, such as heparan sulfate. When a large amount of recombinant HGF is administered intravenously, c-Met levels in the liver decrease, resulting in the reduction of internalization efficiency. In cases of liver damage, plasma HGF levels are likely to increase, not only because of the up-regulation of HGF, but also because of the lower clearance of HGF in the liver.

3. Alteration of serum HGF levels in normal conditions

HGF levels are altered by various factors, such as aging and pregnancy. For example, serum HGF levels in females are 0.36 ng/ml at 10 years of age, increase to 0.39 ng/ml at 20–29 years of age, and decrease with aging to 0.26 ng/ml at 50 (Table 1) [44–47]. There are small differences in HGF levels between males and females: the levels are 0.33 ng/ml in females and 0.29 ng/ml in males at 40–49 years of age (Table 1). Serum HGF levels increase throughout pregnancy from 0.30 ng/ml in the early pregnancy to 0.41 ng/ml in mid-gestation and to 0.48 ng/ml in the late stage of pregnancy (Table 2) [48]. These data suggest the importance of physiological changes in HGF levels in age, sex, and pregnancy.

4. Relationships between HGF levels and diseases, disease stages, and the prognosis for diseases: clinical relevance of HGF levels

Circulating HGF levels change in the presence of different diseases and the correlation between HGF levels, disease parameters, and disease stages are evident. In diseases such as cancer, a correlation between HGF levels and prognosis has been reported (Tables 3A and B).

Table 1
Alteration of HGF levels in serum during aging and by sex

Age (years)	Serum HGF level in healthy controls (ng/ml)		Reference
	Females	Males	
10–19	0.36 ± 0.16	0.35 ± 0.25	[147]
20–29	0.39 ± 0.25	0.37 ± 0.22	
30–39	0.37 ± 0.19	0.33 ± 0.19	
40–49	0.33 ± 0.17	0.29 ± 0.17	
50–59	0.26 ± 0.17	0.29 ± 0.15	

Table 2
Alteration of HGF levels during pregnancy

A

Stage of pregnancy	Serum HGF level in pregnancy (ng/ml)	Reference
Early	0.3	[44]
Middle	0.41 ± 0.21	
End	0.48 ± 0.25	

B

Stage of pregnancy	Amniotic fluid HGF level in pregnancy (ng/ml)	Reference
Early	15 ± 8	[44] ([45])
Middle	48 ± 23	
End	6 ± 3	

C

Stage of pregnancy	Cord vessel HGF level in pregnancy (ng/ml)	Reference
<37 weeks	0.78 (0.46–1.03)	[48]
>37 weeks	1.11 (0.78–1.45)	

A. HGF level in serum. B. HGF level in amniotic fluid. C. HGF level in Cord vessels.

4.1. Liver disease

4.1.1. Serum HGF levels in various hepatic diseases

Serum HGF levels are significantly higher in patients with acute and chronic hepatitis compared with findings in normal controls [49,50]. The levels increase in patients with acute hepatic failure, and are increased 36-fold compared with findings in patients with acute hepatitis. The data for patients with acute hepatitis correlate significantly with serum bilirubin and γ-GTP levels and with the tissue activation index in patients with chronic hepatitis, thereby reflecting histological inflammation and tissue fibrosis [49]. Serum HGF levels in the presence of chronic hepatitis (CH), liver cirrhosis (LC), or hepatocellular carcinoma (HCC) are 0.40, 1.05, and 1.06 ng/ml, respectively. That is significantly higher than in controls (Table 3A). Serum HGF shows a positive correlation with C-reactive protein (CRP) and a negative correlation with albumin. However, no relationship between HGF and alpha2-microglobulin has been observed [51]. Serum HGF levels in patients with hepatitis C are highest in patients with acute hepatitis (AH) and levels tend to be higher in patients with LC

Table 3A
HGF levels in various diseases (selected diseases)

Disease	HGF level (ng/ml; ng/mg)	Reference
Serum		
Normal	0.27 ± 0.08	[50]
Alcoholic liver cirrhosis	0.78	[148] ([53])
Acute hepatitis	0.45 ± 0.23	[50] ([52])
Chronic hepatitis	0.40 ± 0.16	
Hepatic cirrhosis	1.05 ± 0.64	
Hepatocarcinoma	1.06 ± 1.45	
Primary bilious cirrhosis	0.44 ± 0.22	
Fulminant hepatitis	16.40 ± 14.67	
Liver transplantation with uneventful postoperative recovery	0.33 ± 0.04	[149]
Liver transplantation with abnormally elevated PT	2.01 ± 0.99	
Angina	0.3 ± 0.1	[60]
Myocardial infarction (6 h)	10.5 ± 9.1	
Myocardial infarction (6–12 h)	6.8 ± 4.6	
Hypertension (WHO stage I)	0.48 ± 0.03	[150]
Hypertension (WHO stage II, III)	0.88 ± 0.1	
Patients with arteriosclerotic lesions	0.35 ± 0.11	[151]
Acute-phase acute renal failure (ARF)	0.55 ± 0.24	[152]
Chronic tubulointerstitial nephritis	0.44 ± 0.37	
Chronic renal failure (non-dialysis case)	0.33 ± 0.1	[79]
Chronic renal failure (less than one year of dialysis)	0.33 ± 0.13	
Chronic renal failure (5–10 years of dialysis)	0.45 ± 0.13	
Acute renal rejection after transplantation	2.17 ± 1.14	[153]
Peak serum HGF in good renal allograft function	2.48 – 5.63	[154]
Interstitial pneumonia	1.16 ± 0.22 ($P<0.01$)	[54]
Bacterial pneumonia	0.96 ± 0.27 ($P<0.01$)	
Pulmonary fibrosis	0.34 ± 0.002 ($P<0.001$)	[57]
Mild and moderate acute pancreatitis	0.63 ± 0.06	[57]

Table 3A (*continued*)

Disease	HGF level (ng/ml; ng/mg)	Reference
Serum		
Severe acute pancreatitis	2.30 ± 0.61	
Clinical presentation before insulin treatment	0.74 ± 0.14	[154] ([156])
Newly diagnosed type 1 diabetes (diabetes duration 1/2–3 years)	0.78 ± 0.40	
Long-standing type 1 diabetes without renal involvement	0.86 ± 0.42	
Long-standing type I diabetes with renal involvement	0.79 ± 0.27	
Polymyositis (PM)	0.63 ± 0.11	[157]
Dermatomyositis (DM)	0.58 ± 0.07	
Inactive SLE	0.788	[158]
Active SLE	1.02	
Ulcerative colitis	1.384 ± 0.107	[159]
Crohn's disease	1.439 ± 0.084	
HELLP syndrome	1.79 ± 0.35	[160]
Bronchoalveolar lavage fluid (BALF)		
Normal (control)	0.23 ± 0.09	([57]) [58]
Idiopathic pulmonary fibrosis (IPF)	0.77 ± 0.88 ($P<0.001$)	
Rheumatoid arthritis (RA)	0.50 ± 0.64 ($P<0.001$)	
Sarcoidosis	0.41 ± 0.61 ($P<0.05$)	
Cerebral cortex		
Normal (average 70 years old)	9.60 ± 4.62	[161]
Alzheimer's disease (average 78.7 years old)	33.7 ± 18.47	
Progressive Parkinson's disease (average 78.5 years old)	20.23 ± 13.55	
Huntington's disease (average 73.8 years old)	36.15 ± 11.98	
Cerebrospinal fluid (CSF)		
Normal	0.346 ± 0.126	[162]
Aseptic meningitis	0.419 ± 0.07	[162]
Bacterial meningitis	6.101 ± 5.20	
Amyotrophic lateral sclerosis	0.58	[91]
Urine		
Normal	19.3 ± 7.1	[78,163]
Acute tubular necrosis (ATN) (non-oliguric)	6.9 ± 0.7 (ng/g)	

Table 3A (*continued*)

Disease	HGF level (ng/ml; ng/mg)	Reference
Urine		
Acute tubular necrosis (ATN) (oliguric)	19.1 ± 4.2 (ng/g)	
Bile		
Normal	0.8 ± 0.1	[164]
One day after hepatic resection (non-diabetic case)	4.0 ± 0.4 ($P<0.05$)	
Control	2.16 ± 1.39	[165]
Rhegmatogenous retinal detachment	2.02 ± 0.84	
Proliferative vitreoretinopathy	3.94 ± 2.29	
Vitreous body		
Non-diabetic case	1.6	[155]
Diabetic retinopathy (rubeosis −)	4.2 ($P<0.05$)	
Diabetic retinopathy (rubeosis+)	7.2 ($P<0.01$)	
Synovial fluid		
Osteoarthritis	0.19	[105] ([166])
Bacterial arthritis	0.18	
Rheumatoid arthritis	1.21	
Placenta		
Normal	6.16 ± 3.32	[46]
Toxemia of pregnancy	4.05 ± 1.44 ($P<0.05$)	

and HCC than in those with chronic hepatitis (CH). Furthermore, serum HGF levels reveal high carcinogenic states in chronic hepatitis and liver cirrhosis type C [52]. Induction is due to the increased production of HGF, not only in the liver, but also in distant organs, such as the lung. With the progression of liver damage, clearance of HGF in the liver diminishes. In addition, although patients with LC show a marked increase in serum HGF levels as the molecule is processed from a biologically inactive single-chain precursor form of HGF into the two-chain active form. Levels may be significantly disturbed in the damaged liver, and a single-chain precursor form can become a major form in the serum. In patients with fulminant hepatitis, extremely high serum levels of HGF (16.40 ng/ml) were detected. In such cases, some of the HGF may exist in the form of